

This discussion paper is/has been under review for the journal Atmospheric Chemistry and Physics (ACP). Please refer to the corresponding final paper in ACP if available.

Retrieving tropospheric nitrogen dioxide over China from the Ozone Monitoring Instrument: effects of aerosols, surface reflectance anisotropy and vertical profile of nitrogen dioxide

J.-T. Lin¹, R. V. Martin^{2,3}, K. F. Boersma^{4,5}, M. Sneep⁴, P. Stammes⁴, R. Spurr⁶, P. Wang⁷, M. Van Roozendael⁸, K. Clémer⁹, and H. Irie¹⁰

¹Laboratory for Climate and Ocean-Atmosphere Studies, Department of Atmospheric and Oceanic Sciences, School of Physics, Peking University, Beijing 100871, China

²Department of Physics and Atmospheric Science, Dalhousie University, Halifax, Nova Scotia, Canada

³Atomic and Molecular Physics Division, Harvard, Smithsonian Center for Astrophysics, Cambridge, Massachusetts, USA

⁴Royal Netherlands Meteorological Institute, De Bilt, the Netherlands

⁵Fluid Dynamics Lab, Eindhoven University of Technology, Eindhoven, the Netherlands

⁶RT Solutions Inc., Cambridge MA 02138, USA

ACPD

13, 21203–21257, 2013

Retrieving
tropospheric nitrogen
dioxide over China

J.-T. Lin et al.

Title Page

Abstract

Introduction

Conclusions

References

Tables

Figures

◀

▶

Back

Close

Full Screen / Esc

Printer-friendly Version

Interactive Discussion



⁷IAP/CAS, Institute of Atmospheric Physics, Chinese Academy of Sciences, Beijing, China

⁸BIRA-IASB, Belgian Institute for Space Aeronomy, Brussels, Belgium

⁹Instituut voor sterrenkunde, KU Leuven, Celestijnenlaan 200D, 3001 Heverlee, Belgium

¹⁰Center for Environmental Remote Sensing, Chiba University, 1-33 Yayoi-cho, Inage-ku, Chiba 263-8522, Japan

Received: 2 July 2013 – Accepted: 2 August 2013 – Published: 14 August 2013

Correspondence to: J.-T. Lin (linjt@pku.edu.cn)

Published by Copernicus Publications on behalf of the European Geosciences Union.

ACPD

13, 21203–21257, 2013

Retrieving
tropospheric nitrogen
dioxide over China

J.-T. Lin et al.

Title Page

Abstract

Introduction

Conclusions

References

Tables

Figures

◀

▶

Back

Close

Full Screen / Esc

Printer-friendly Version

Interactive Discussion



Abstract

Retrievals of tropospheric nitrogen dioxide (NO_2) from the Ozone Monitoring Instrument (OMI) are subject to errors in the treatments of aerosols, surface reflectance anisotropy, and vertical profile of NO_2 . Here we quantify the influences over China via an improved retrieval process. We explicitly account for aerosol optical effects (simulated by nested GEOS-Chem at $0.667^\circ \text{lon} \times 0.5^\circ \text{lat}$ and constrained by aerosol measurements), surface reflectance anisotropy, and high-resolution vertical profiles of NO_2 (simulated by GEOS-Chem). Prior to the NO_2 retrieval, we derive the cloud information using consistent ancillary assumptions. We compare our retrieval to the widely used DOMINO v2 product, using as reference MAX-DOAS measurements at three urban/suburban sites in East China and focusing the analysis on the 127 OMI pixels (in 30 days) closest to the MAX-DOAS sites. We find that our retrieval reduces the interference of aerosols on the retrieved cloud properties, thus enhancing the number of valid OMI pixels by about 25 %. Compared to DOMINO v2, our retrieval improves the correlation with the MAX-DOAS data in the day-to-day variability of NO_2 ($R^2 = 0.96$ vs. 0.72). Our retrieved NO_2 columns are about 50 % of the MAX-DOAS data on average. This reflects the inevitable spatial inconsistency between the two types of measurement, uncertainties in MAX-DOAS data, and residual uncertainties in our OMI retrievals related to aerosols and vertical profile of NO_2 . Through a series of tests, we find that excluding aerosol scattering/absorption can either increase or decrease the retrieved NO_2 , with a mean absolute difference by about 20 %. Concentrating aerosols at the boundary layer top enhances the retrieved NO_2 by 8 % on average with a mean absolute difference by 23 %. The aerosol perturbations also affect nonlinearly the retrieved cloud fraction and particularly cloud pressure. Employing various surface albedo datasets alters the retrieved NO_2 by 0–7 % on average. The retrieved NO_2 columns increase when the NO_2 profiles are taken from MAX-DOAS retrievals (by 20 % on average) or TM4 simulations (by 10 %) instead of GEOS-Chem simulations. Our findings are also

Title Page	
Abstract	Introduction
Conclusions	References
Tables	Figures
◀	▶
◀	▶
Back	Close
Full Screen / Esc	
Printer-friendly Version	
Interactive Discussion	



relevant to retrievals of other pollutants (e.g., sulfur dioxide, formaldehyde, glyoxal) from UV-vis backscatter satellite instruments.

1 Introduction

The vertical column densities (VCDs) of tropospheric nitrogen dioxide (NO_2) retrieved from the Ozone Monitoring Instrument (OMI) have been used extensively to analyze emissions of nitrogen oxides (NO_x) from anthropogenic and/or natural sources (Hudman et al., 2010; Mebust et al., 2011; Beirle et al., 2011; Lin, 2012), including the magnitude (Zhao and Wang, 2009; Lin et al., 2010b; Mijling and van der A, 2012), trends (Lin et al., 2010a; Lamsal et al., 2011; Castellanos and Boersma, 2012; Wang et al., 2012; Zhou et al., 2012), and variability (Mijling et al., 2009; Hudman et al., 2010; Yu et al., 2010; Lin and McElroy, 2011). The NO_2 retrievals have also been used to analyze NO_x concentrations near the ground (Lamsal et al., 2008; Novotny et al., 2011). The retrieved changes in NO_x are found to have influenced other pollution such as aerosols (Lin et al., 2010a) and ozone (Walker et al., 2010), and have become a major concern for the atmospheric environment (Richter et al., 2005; Zhang et al., 2012).

The retrieval of tropospheric NO_2 VCD from OMI is done by dividing the tropospheric slant column density (SCD) by the tropospheric air mass factor (AMF) (Boersma et al., 2011). (Hereafter we will focus the analysis in the troposphere.) The AMF is derived by radiative transfer modeling driven by ancillary assumptions on surface reflectance (Rs), surface pressure (Ps), aerosol characteristics, cloud fraction (CF), cloud pressure (CP), and vertical profile of NO_2 .

The calculation of AMF provides the dominant source of errors in the retrieved NO_2 columns over polluted areas (Boersma et al., 2007). In particular, current representative OMI products DOMINO v2 (Boersma et al., 2011) and OMNO2 v2 (Bucsela et al., 2013) do not explicitly account for the effect of aerosols on the solar radiation. Rather, these retrievals assume that the cloud correction accounts for the effect of aerosols, as the OMI cloud retrieval provides effective cloud parameters sensitive to aerosol bur-

Title Page

Abstract

Introduction

Conclusions

References

Tables

Figures

|◀

▶|

◀

▶|

Back

Close

Full Screen / Esc

Printer-friendly Version

Interactive Discussion



Title Page	
Abstract	Introduction
Conclusions	References
Tables	Figures
◀	▶
◀	▶
Back	Close
Full Screen / Esc	
Printer-friendly Version	
Interactive Discussion	

dens (Boersma et al., 2011). Since aerosols affect the radiation field in retrieving both clouds (Boersma et al., 2011) and NO₂ (Leitão et al., 2010), the net effect on the retrieved NO₂ columns is unclear. This aerosol issue is particularly significant over East China due to its high aerosol loadings (Lin et al., 2010a; Cheng et al., 2013). Martin (2008) recommended addressing this issue by retrieving cloud fields that account for the effects of aerosols. In addition, the DOMINO and OMNO2 products also assume Lambertian surface with no dependence of surface reflectance on the geometry of the light path (Boersma et al., 2011; Bucsela et al., 2013). They adopt the vertical profile of NO₂ simulated by coarse-resolution global chemical transport models (CTMs), TM4 at 3° lon × 2° lat for DOMINO v2 and GMI at 2.5° lon × 2° lat for OMNO2 v2, which are unable to capture the variability of NO₂ at smaller scales. Russell et al. (2011) found differences in retrieved NO₂ columns by –75–10 % for OMI pixels around California in June 2008 when adopting NO₂ profiles from a WRF-Chem simulation at a resolution of 4 km × 4 km instead of a GEOS-Chem simulation at 2.5° lon × 2° lat; they did not separate the effect of model resolution from the effects of other model setups. Furthermore, DOMINO and OMNO2 adopt the cloud information from the OMCLDO2 cloud retrieval (Acarreta et al., 2004; Sneep et al., 2008) with consistent assumptions on reflective properties (Earth's surface and clouds are treated as Lambertian surfaces) and surface albedo (from Kleipool et al., 2008), but with differences in the assumed surface pressure (see more discussion in Sects. 2.2 and 3). Research has found potentially large errors in the NO₂ products in comparison to aircraft measurements (Bucsela et al., 2008; Hains et al., 2010). For China, such evaluation is rare (Irie et al., 2012; Ma et al., 2013), and the effects of individual parameters have not been quantified.

Here we evaluate the effects of aerosols, Rs, and vertical profile of NO₂ on the retrieval of tropospheric NO₂ columns over East China. For this purpose, we improve upon DOMINO v2 (hereafter referred to as DOMINO-2) by enhancing the assumptions on Ps, Rs, aerosol optics, cloud properties, and vertical profile of NO₂. We calculate the tropospheric AMFs independently and adopt the tropospheric SCDs from DOMINO-2. Prior to the retrieval of NO₂, we derive the cloud information through the O₂-O₂ method



(Acarreta et al., 2004; Sneeep et al., 2008) but using improved ancillary parameters (Ps, Rs, aerosols, pressure levels, temperature profiles) consistent with our NO₂ retrieval. We compare our retrieval to DOMINO-2 using as reference the ground-based MAX-DOAS measurements from three urban/suburban sites in East China in various months of 5 2006, 2008, 2009 and 2011. We perturb the ancillary parameters to test their influences on the retrievals of clouds and NO₂ columns. Our analysis is focused on the OMI measurements consistent with the MAX-DOAS data.

Section 2 describes the NO₂ products retrieved from OMI and MAX-DOAS and presents the criteria for selecting suitable OMI and MAX-DOAS measurements for 10 comparison. Section 3 compares the ancillary parameters employed by DOMINO-2 to those by our retrieval. Section 4 compares DOMINO-2 and our OMI retrieval to the NO₂ columns retrieved from MAX-DOAS. Section 5 further evaluates the effects of individual ancillary parameters on the retrievals of clouds and NO₂ columns from OMI, through a series of sensitivity tests. Section 6 concludes this study.

15 2 Retrievals of NO₂ and criteria for data selection

2.1 MAX-DOAS measurements

The MAX-DOAS measurements were conducted at three urban/suburban sites in East China, one at the Institute of Atmospheric Physics (IAP), Chinese Academy of Sciences (CAS) in urban Beijing, one in Xianghe County to the southeast of Beijing, and one in 20 Tai'An City. Figure 1 shows the locations of these sites with respect to the NO₂ columns in July 2008 retrieved from DOMINO-2. More information about the sites is described in Table 1.

The instrument operated in Beijing and Xianghe has been designed at BIRA-IASB and is described extensively by Clémer et al. (2010). It is a dual-channel system composed of two thermally regulated grating spectrometers covering the ultraviolet and visible wavelength ranges (300–390 nm and 400–720 nm, respectively) by means of 25

Retrieving tropospheric nitrogen dioxide over China

J.-T. Lin et al.

[Title Page](#)

[Abstract](#)

[Introduction](#)

[Conclusions](#)

[References](#)

[Tables](#)

[Figures](#)

◀

▶

◀

▶

[Back](#)

[Close](#)

[Full Screen / Esc](#)

[Printer-friendly Version](#)

[Interactive Discussion](#)



**Retrieving
tropospheric nitrogen
dioxide over China**

J.-T. Lin et al.

[Title Page](#)[Abstract](#)[Introduction](#)[Conclusions](#)[References](#)[Tables](#)[Figures](#)[|◀](#)[▶|](#)[◀](#)[▶|](#)[Back](#)[Close](#)[Full Screen / Esc](#)[Printer-friendly Version](#)[Interactive Discussion](#)

low-noise cooled CCD detectors. Scattered light is collected at various elevation angles within a field of view of about 0.5° by a telescope mounted on a commercial sun tracker. The received light is guided to the spectrometers through depolarizing optical fiber bundles. The telescope points towards a fixed azimuth direction (north). A full MAX-DOAS scan, which requires ~ 15 min, comprises nine elevation angles at 2° , 4° , 6° , 8° , 10° , 12° , 15° , 30° , and 90° (zenith).

The instrument at Tai'An employs a miniaturized ultraviolet/visible spectrometer (B&W TEK Inc., BTC111), a single telescope, and a movable mirror. It measures scattered sunlight sequentially every 30 min at five elevation angles: 5° , 10° , 20° , 30° , and 90° . The telescope points to a fixed azimuth direction (north). The spectral resolution is about 0.4–0.5 nm for the fitting window of 460–490 nm. More information is given by Irie et al. (2008) and Irie et al. (2012).

For all sites, the VCD of NO_2 is retrieved from the radiation measurements around 477 nm. A profile approach based on an optimal estimation scheme (Rodgers, 2000) is taken that results in a companion vertical profile of NO_2 (Irie et al., 2012; Hendrick et al., 2013). The vertical profile may not represent the true distribution of NO_2 because the degrees of freedom for signal (DFS) is only about 2 (Hendrick et al., 2013) or less (Irie et al., 2011) from the retrieval process. Compared to space-based remote sensing, the MAX-DOAS measurements are insensitive to surface reflectance and are subject to better cloud screening. The total retrieval uncertainty on the tropospheric NO_2 column has been estimated at 11 % for the Beijing and Xianghe sites (Hendrick et al., 2013) and 14 % for the Tai'An site (Irie et al., 2012). These uncertainty estimates do not account for the spatial representativeness of MAX-DOAS measurements, an important factor when comparing to satellite retrievals that cover a larger area (see Sects. 2.4 and 5.6).

Prior to the retrieval of NO_2 , the MAX-DOAS remote sensing data are used to derive aerosol optical depth (AOD) and aerosol extinction profile (Clémér et al., 2010; Irie et al., 2011). We employed the AOD results at the Tai'An site to constrain the respective aerosol information in retrieving clouds and NO_2 columns from OMI (see Sect. 2.3). The

retrieved aerosol extinction profile was not used considering its low DFS at 2.1 ± 0.6 (Irie et al., 2011).

2.2 DOMINO-2

For DOMINO-2, the AMF is interpolated from a pre-calculated look-up table (LUT) derived from the Doubling-Adding KNMI (DAK v3.0) radiative transfer model (RTM). The LUT provides layer AMFs (i.e., the sensitivity of SCD to VCD in individual atmospheric layers) that are determined by surface albedo (A_s), P_s , CF, CP, atmospheric pressure level, and the geometry of the light path. Table 2 summarizes the ancillary parameters used in deriving DOMINO-2.

DOMINO-2 adopts the monthly A_s data averaged from the OMI measurements between October 2004 and October 2007 (OMLER v1; Kleipool et al., 2008), not accounting for the effect of surface reflectance anisotropy. These A_s values are affected by the presence of aerosols (Herman et al., 2001; Kleipool et al., 2008). For a given ground pixel of OMI, the surface pressure is interpolated to the pixel center from TM4 simulations on a 3° lon \times 2° lat grid, and subsequently corrected for differences between the corresponding effective ground elevation and the high-resolution elevation obtained from the DEM_3KM database (Boersma et al., 2011). The vertical profile of NO_2 is adjusted subsequently, by maintaining the volume mixing ratios (VMRs) of NO_2 in the individual layers so that the profile shape is not changed. The detailed formulation of the adjustments is presented by Zhou et al. (2009) and Boersma et al. (2011).

DOMINO-2 takes the cloud fraction and cloud pressure information from the OMCLDO2 v1.1.1.3 dataset (Acarreta et al., 2004; Sneep et al., 2008). (Hereafter the version number of OMCLDO2 is dropped for simplicity.) Table 3 summarizes the ancillary parameters used for deriving OMCLDO2. Compared to DOMINO-2, OMCLDO2 assumes a time-invariant relationship between pressure and height (i.e., the midlatitude summer profile from Anderson et al., 1986) and uses the pixel-specific ground elevation to determine the respective P_s . The effect of the inconsistent treatments of P_s between DOMINO-2 and OMCLDO2 is analyzed in Sects. 3 and 4.1.

Title Page	
Abstract	Introduction
Conclusions	References
Tables	Figures
◀	▶
◀	▶
Back	Close
Full Screen / Esc	
Printer-friendly Version	
Interactive Discussion	



Retrieving tropospheric nitrogen dioxide over China

J.-T. Lin et al.

Title Page

Abstract

Introduction

Conclusions

References

Tables

Figures

◀

▶

◀

▶

Back

Close

Full Screen / Esc

Printer-friendly Version

Interactive Discussion



The retrieval processes of both DOMINO-2 and OMCLDO2 do not explicitly account for the effect of aerosols (scattering, absorption, and vertical profile). The cloud fraction and cloud pressure retrieved from OMCLDO2 are thus considered as “effective” parameters that may include partial information about the presence of aerosols (Boersma et al., 2011). The implicit treatment of aerosols affects the retrieval of NO₂ over East China, given its high aerosol concentrations.

2.3 Our reference retrieval

Using the LIDORT v3.6 RTM (Spurr, 2008), we improved the AMF formulation by Palmer et al. (2001), Martin et al. (2002, 2003, 2006) and O’Byrne et al. (2010) to AMFv6 that simultaneously accounts for the coupled effects of aerosols and clouds on the NO₂ retrieval, and for the angular distribution of surface reflectance. This code has the capability to calculate independently the tropospheric AMFs of NO₂ for individual OMI pixels with no use of a LUT. We derived the VCDs of NO₂ by dividing the tropospheric SCDs from DOMINO-2 by the newly calculated AMFs. Prior to the retrieval of NO₂, we derived the cloud information (CF and CP) based on the top-of-atmosphere reflectance and the O₂-O₂ SCD data from OMCLDO2 (Acarreta et al., 2004; Sneed et al., 2008), using ancillary parameters that are consistent with the NO₂ retrieval. Tables 2 and 3 summarize the ancillary parameters used in our retrieval processes for NO₂ and clouds, respectively. The retrieval here is referred to as our “reference retrieval” (Case 0 in Table 4), to be distinguished from the sensitivity tests throughout the text (Cases 1–17).

For Rs, our reference retrieval accounts for the effect of surface bi-directional reflectance distribution function (BRDF) (Zhou et al., 2010). We adopted the MCD43C2 dataset (Lucht et al., 2000) from the Moderate Resolution Imaging Spectroradiometer (MODIS) that provides the coefficients for three kernels (isotropic, volumetric and geometric) determining the BRDF at 440 nm. MCD43C2 provides 16 day average coefficients for every 8 days of a year on a 0.05° lon × 0.05° lat grid (the first file contains the average values over 1–16 January, the second file represents 9–24 January, etc.).

To fill the missing values, we interpolated the data temporally using the adjacent two datasets, spatially with the surrounding 5×5 gridcells, temporally using the respective datasets in the adjacent two years, and then temporally using the 2005–2011 average values representing the same days. The interpolation was done in the above order, and was exited once the missing value had been filled. We then conducted spatial smoothing (5×5 gridcells) on the coefficients to remove the influence of ice or snow that may not have been fully eliminated in MCD43C2. As a final step, we derived the kernel coefficients for an OMI pixel in a given day from the high-resolution dataset by spatial mapping and temporal interpolation.

Our reference retrieval obtains the Ps and NO₂ profiles from the nested GEOS-Chem model (0.667° lon $\times 0.5^\circ$ lat) with further adjustments in accordance to the pixel-specific surface elevation as done for DOMINO-2. See Appendix A for a brief model description. For surface elevation, we adopted the GMTED2010 dataset at 30 arc-seconds (http://topotools.cr.usgs.gov/GMTED_viewer/). GEOS-Chem simulates vertical mixing in the planetary boundary layer (PBL) fairly well (Lin and McElroy, 2010). Compared to TM4, the nested GEOS-Chem has much higher resolution, thus improving the representation of topography, emissions, and the nonlinear chemistry. We obtained the model outputs at the local time of OMI pixels.

Our reference retrieval explicitly accounts for the effect of aerosol optics by including in the RTM calculation the vertical profiles of aerosol extinction coefficient (EC), single scattering albedo (SSA), and phase functions. We adopted the temporally and spatially varying aerosol information at the local time of OMI pixels from the nested GEOS-Chem simulation (Lin, 2012). See Appendix A for descriptions of the aerosol simulation. GEOS-Chem captures the spatial distribution of AOD at 550 nm over East China in 2006 observed from MODIS, with a positive bias in winter and a negative bias in summer on average (Lin et al., 2012). Comparisons with the AOD measurements from the AErosol RObotic NETwork (AERONET) at the overpass time of OMI show a correlation of 0.74 at Beijing IAP (mean bias = -0.12 , intercept = -0.18 , slope = 1.08) and 0.75 at Xianghe (mean bias = -0.07 , intercept = -0.05 , slope = 0.97) for 2006. To

Title Page	
Abstract	Introduction
Conclusions	References
Tables	Figures
◀	▶
◀	▶
Back	Close
Full Screen / Esc	
Printer-friendly Version	
Interactive Discussion	



further constrain the modeled aerosol optics, we employed the AOD measurements from AERONET, MODIS, and MAX-DOAS. We modified the simulated concentrations of aerosols based on the amount of simulated relative to the observed AOD; the same wavelength was ensured in comparing each pair of model and observation (476 nm at 5 Tai’An and 550 at Beijing IAP and Xianghe; see below). For the Tai’An site, we used the AOD data at 476 nm retrieved from the MAX-DOAS measurements (Irie et al., 2011). For IAP and Xianghe (Liu et al., 2007), we used the AERONET data at 550 nm at the hour of the MAX-DOAS measurements. For seven days (34 pixels) without AERONET data, we used the MODIS AOD data at 550 nm from the MYD04 Collection 5/5.1 level- 10 2 product (Remer et al., 2008). For a given day, the MYD04 data were averaged over all valid values within 0.25° of the respective MAX-DOAS sites. The MODIS AOD are affected by cloud contamination and errors in surface reflectance (Wang et al., 2010; Hyer et al., 2011). The consequent effects on our cloud and NO₂ retrievals are small compared to the effects of potential errors in modeled SSA and vertical distribution of 15 aerosols. After the aerosol adjustments, the resulting AOD at 550 nm ranges from 0.07 to 2.23 with a mean value of 0.61 for the 127 OMI pixels complying with our spatial constraints (see Sect. 2.4). The SSA at 550 nm as simulated by GEOS-Chem is 0.934 on average (min = 0.870, max = 0.986), reflecting the high concentrations of black carbon in East China (Yang et al., 2011). The GEOS-Chem aerosol vertical profile generally reproduces that observed by the Cloud-Aerosol Lidar with Orthogonal Polarization (CALIOP) over East Asia, with a tendency for GEOS-Chem to underestimate the abundance of aerosols in the free troposphere (Ford and Heald, 2012; van Donkelaar et al., 2013). In calculating the AMFs of O₂-O₂ and NO₂, we adjusted the aerosol optics to 20 the respective wavelengths (475 nm for O₂-O₂ and 438 nm for NO₂).

2.4 Criteria for selecting OMI and MAX-DOAS data

As the MAX-DOAS sites are located in the urban or suburban areas, the spatial variability of NO₂ needs to be considered in selecting suitable OMI and MAX-DOAS data for comparison. Parameters that can be used to adjust the spatial consistency be-

Title Page

Abstract

Introduction

Conclusions

References

Tables

Figures

◀

▶

◀

▶

Back

Close

Full Screen / Esc

Printer-friendly Version

Interactive Discussion



tween the space- and ground-based measurements include the viewing zenith angle (VZA) of OMI and the distance from the OMI pixel center to the respective MAX-DOAS site (hereafter referred to as pixel-center distance). For our analysis, the distance is restricted to be shorter than 25 km and the VZA smaller than 30° , unless stated otherwise.
5 This, together with the constraints for temporal consistency, row anomaly, ground conditions and cloud interference discussed below, results in 127 pixels of OMI over 30 days with suitable OMI and MAX-DOAS data. A total of 98 pixels (in 23 days) correspond to the IAP site, 27 pixels (in 6 days) correspond to the Tai'An site, and 2 pixels (in 1 day) correspond to the Xianghe site. Under stricter spatial constraints, the number
10 of days with suitable data decreases significantly and does not allow for a meaningful analysis. The dependence on distance and VZA of the comparison between OMI and MAX-DOAS data is discussed in Sect. 4. As detailed in Sect. 5.6, such spatial constraints cannot fully eliminate the spatial inconsistency between MAX-DOAS and OMI measurements.

15 Temporally, MAX-DOAS measures NO_2 much more frequently than OMI throughout the course of a day. In many days, it observes rapid changes in NO_2 within a short time period. To reduce the effect of the temporal variation of NO_2 in comparing the ground- and space-based measurements, here the measurement from an OMI pixel is considered to have a temporally consistent counterpart from MAX-DOAS only if: (1)
20 there exist two or more MAX-DOAS data within 1.5 h of the time of the OMI pixel, and (2) the standard deviation of these MAX-DOAS data does not exceed 20 % of their mean value. In this case, the mean value of the MAX-DOAS data points is paired with the OMI value for comparison.

25 In addition, we excluded the OMI pixels affected by row-anomaly, icy/snowy ground, or high cloud coverage. DOMINO-2 restricts valid NO_2 data to the pixels with cloud radiance fractions (CRFs) below 0.5. It also implicitly excludes the pixels with high aerosol loadings, since its cloud information is influenced by the presence of aerosols. This may not be desirable for aerosol-polluted regions such as East China, particularly when the effects of aerosols can otherwise be characterized. By comparison, our

Title Page

Abstract

Introduction

Conclusions

References

Tables

Figures

◀

▶

◀

▶

Back

Close

Full Screen / Esc

Printer-friendly Version

Interactive Discussion



reference retrieval explicitly accounts for the effect of aerosol optics, thus providing information that is more specific to clouds. For example, there is a heavy aerosol loading near the IAP site on December 28, 2008 with the AERONET AOD close to 2. For this day, our reference retrieval suggests low cloud coverage in an OMI pixel with a CRF of 6 %, in contrast to the CRF at 55 % suggested by DOMINO-2. Detailed comparison of the cloud information is presented in Sect. 3. Therefore, we used the CRF values derived from our reference retrieval to determine the OMI pixels with low cloud coverage ($\text{CRF} \leq 0.5$) in comparing OMI to MAX-DOAS data. Had the CRFs from DOMINO-2 been used for constraint, the number of pixels would have reduced from 127 (in 30 days) to 98 (in 24 days).

3 Evaluating ancillary parameters for deriving DOMINO-2 and our reference retrieval

Unlike DOMINO-2, our reference retrieval accounts for surface BRDF. Here we used the respective bi-directional reflectance factor (BRF) to illustratively compare with the OMI albedo adopted by DOMINO-2. We neglected the scale factor π when deriving the BRF from the BRDF (Lucht et al., 2000). Figure 2a shows that the BRF is in the same range as the OMI albedo, 0.03–0.08, but the two data correlate poorly with the coefficient of determination (R^2) below 0.05. Also, the MODIS BRF varies from one pixel to another more significantly than the OMI albedo (note the apparent horizontal lines in Fig. 2a). The OMI albedo is larger the BRF by 0.023 averaged over the pixels.

The Ps adjustment in deriving DOMINO-2 leads to unrealistically high Ps for most of the 127 pixels analyzed here, an apparent result of the likely overestimate in the TM4 Ps data. The adjusted Ps exceeds 1050 hPa in 97 of the 127 pixels and exceeds 1100 hPa in 31 pixels (Fig. 2b). It exceeds the Ps assumed in OMCLDO2 by 57.7 hPa averaged over the 127 pixels and by 80.0 hPa for the 100 pixels near IAP or Xianghe. For the pixels near the IAP or Xianghe sites, the adjusted Ps is larger than the Ps observed from the Nanjiao (116.47°E , 39.80°N , 31 m) ground meteorological station

Title Page	
Abstract	Introduction
Conclusions	References
Tables	Figures
◀	▶
◀	▶
Back	Close
Full Screen / Esc	
Printer-friendly Version	
Interactive Discussion	



Title Page

Abstract

Introduction

Conclusions

References

Tables

Figures

◀

▶

◀

▶

Back

Close

Full Screen / Esc

Printer-friendly Version

Interactive Discussion



in the southeast of urban Beijing (mean bias = 75.2 hPa, $R^2 = 0.35$). Further analysis shows positive biases in the DOMINO-2 Ps data over various regions of East China with no obvious dependence on land use types (J.-T. Lin et al., Improved retrieval of the tropospheric NO₂ seasonality from the Ozone Monitoring Instrument, 2013). By comparison, the Ps derived in our reference retrieval is consistent with the observed Ps at Nanjiao (mean bias = -9.1 hPa, $R^2 = 0.65$).

Figure 2c–e compares the CF, CP and CRF between DOMINO-2 and our reference retrieval. As mentioned in Sect. 2.2, the DOMINO-2 CF and CP are taken from OM-CLDO2. The CFs and CRFs for DOMINO-2 are larger than those derived from our reference retrieval for most pixels (0.100 vs. 0.063 for CF and 0.326 vs. 0.180 for CRF), as explained by the different treatments concerning aerosols. On the other hand, our reference retrieval suggests higher CP than DOMINO-2 (OMCLDO2) with a mean difference by about 30 hPa.

For the assumed vertical profile of NO₂, our reference retrieval differs from DOMINO-2 due to the differences between the coarse-resolution TM4 and high-resolution GEOS-Chem simulations as well as the different adjustments in accordance to the Ps. Figure 3b presents an illustrative example of the vertical profiles assumed by DOMINO-2 and by our reference retrieval for a pixel on December 28, 2008. Compared to our reference retrieval, the NO₂ profile in DOMINO-2 for this pixel is associated with much higher Ps and also assumes NO₂ to be more concentrated near the ground. The differences contribute partly to the much lower AMF in DOMINO-2 than our reference retrieval (0.32 vs. 0.90).

4 Evaluating DOMINO-2 and our reference retrieval using MAX-DOAS measurements

We used scatter plots and the reduced major axis (RMA) regression to evaluate the consistency between OMI and MAX-DOAS data. Our analysis emphasizes the R^2 of the regression that evaluates the variability of NO₂ retrieved from OMI; the slope is

Retrieving tropospheric nitrogen dioxide over China

J.-T. Lin et al.

[Title Page](#)[Abstract](#)[Introduction](#)[Conclusions](#)[References](#)[Tables](#)[Figures](#)[|◀](#)[▶|](#)[◀](#)[▶|](#)[Back](#)[Close](#)[Full Screen / Esc](#)[Printer-friendly Version](#)[Interactive Discussion](#)

Figure 5 shows the dependence of the consistency between daily OMI and MAX-DOAS data on the spatial constraints by pixel-center distance (from 25 km to 50 km) and VZA (from 30° to unlimited). For both DOMINO-2 and our reference retrieval, loosening the distance constraint results in a monotonic reduction in the slope (from the RMA regression) with respect to the MAX-DOAS data (Fig. 5a and c).

With a given VZA constraint, the slope reduces by 0.09–0.31 from distance \leq 25 km to distance \leq 50 km. This is consistent with the findings by Irie et al. (2012) for the polluted Yokosuka site in Japan. Varying the VZA constraint does not lead to a monotonic change in the slope. For our reference retrieval, the slope varies from 0.36 to 0.51 across the range of the spatial constraints, and is consistently smaller than the slope for DOMINO-2 (0.74–1.10). However, our reference retrieval correlates much better with the MAX-DOAS data, with R^2 of 0.78–0.96 compared to 0.63–0.79 for DOMINO-2 (Fig. 5b and d).

4.1 Understanding the differences between DOMINO-2 and MAX-DOAS

That the mean magnitude of NO_2 columns derived from DOMINO-2 is close to the MAX-DOAS value is coincidental and is influenced by the treatments of Ps and clouds by DOMINO-2. As analyzed in Sect. 3, DOMINO-2 overestimates the observed Ps by 75.2 hPa on average and adjusts the pressure dependence of NO_2 accordingly. It adopts the CP from OMCLDO2 (that assumes lower Ps) without additional adjustments. Thus it puts more NO_2 below the cloud top, consequently lowering the AMF. In addition, DOMINO-2 adopts the OMCLDO2 CF data which are overestimated due to the influence of aerosols. This further enhances the sensitivity to the treatments of Ps and CP. When we changed the retrieval process of Case 1 by adopting the Ps from OMCLDO2 (Case 2 in Table 4), the resulting NO_2 columns were lower than Case 1 by 27 % averaged over the 127 pixels; and they exceeded our reference retrieval (Case 0) by 17 % only.

To put into perspective the correlation between DOMINO-2 and MAX-DOAS, we deduced the tropospheric VCD retrieved from OMI as the geometric VCD (gVCD) divided by the normalized AMF (nAMF) (see Eq. 1). The nAMF is the AMF divided by the ge-

Title Page

Abstract

Introduction

Conclusions

References

Tables

Figures

◀

▶

◀

▶

Back

Close

Full Screen / Esc

Printer-friendly Version

Interactive Discussion



ometric AMF (gAMF) that only accounts for the solar zenith angle (SZA) and VZA of the light path. Thus the nAMF represents the overall effect of non-geometry ancillary parameters in retrieving the VCD of NO₂ from OMI. The OMI gVCD strongly correlates to the MAX-DOAS VCD: the R^2 amounts to 0.82 for the 127 pixel-specific values and 0.87 for the 30 daily data. The weaker correlation between DOMINO-2 and MAX-DOAS ($R^2 < 0.75$) indicates that the retrieval process of DOMINO-2 does not improve the variability of AMF upon a geometric AMF for the pixels investigated here. This is in contrast to the improved correlation with MAX-DOAS by our reference retrieval ($R^2 > 0.90$).

$$\text{VCD} = \frac{\text{SCD}}{\text{AMF}} = \frac{\text{SCD/gAMF}}{\text{AMF/gAMF}} = \frac{\text{gVCD}}{\text{nAMF}}$$

(1)

10 gAMF = sec(SZA) + sec(VZA)

5 Effects of aerosols, surface reflectance, and vertical profile of NO₂ in retrieving NO₂ columns from OMI

Analyses of Cases 0–2 in Sect. 4 provide the overall effect of ancillary assumptions in retrieving NO₂ columns from OMI. In this section, we tested the individual effects of aerosols, Rs and vertical profile of NO₂ by perturbing the parameters during the retrieval process of Case 0. We also retrieved the cloud information with the perturbed parameters prior to the derivation of NO₂. Table 4 describes the various perturbations (Cases 3–17). Here we present the resulting effects for the 127 pixels complying with the spatial constraints of pixel-center distance ≤ 25 km and VZA $\leq 30^\circ$. We use the

[Title Page](#)[Abstract](#)[Introduction](#)[Conclusions](#)[References](#)[Tables](#)[Figures](#)[◀](#)[▶](#)[Back](#)[Close](#)[Full Screen / Esc](#)[Printer-friendly Version](#)[Interactive Discussion](#)

following statistics to quantify the effects of ancillary parameters:

$$\begin{aligned} \text{MD} &= \frac{1}{n} \sum_{i=1}^n B_i - A_i \\ \text{MAD} &= \frac{1}{n} \sum_{i=1}^n |B_i - A_i| \\ \text{NMD} &= \frac{\text{MD}}{\frac{1}{n} \sum_{i=1}^n A_i} \\ 5 \quad \text{NMAD} &= \frac{\text{MAD}}{\frac{1}{n} \sum_{i=1}^n A_i} \end{aligned} \tag{2}$$

Here MD denotes mean difference and MAD denotes mean absolute difference. NMD and NMAD represent the normalized MD and MAD, respectively. The subscript i indicates a pixel from $n = 127$ pixels. A_i denotes the values from Case 0 and B_i the other cases. The results are summarized in Fig. 6 for Rs, Ps, AOD, cloud properties, the AMF of NO₂, and the VCD of NO₂. The correlation between these sensitivity cases and Case 0 is presented in Fig. 7 for the AMF and VCD of NO₂.

5.1 Effects of surface reflectance

In retrieving the cloud information, an increase in Rs will enhance the AMF of O₂-O₂ that is compensated by a decrease in CP (Fig. 8). The increased Rs also enhances the reflectance at top-of-atmosphere (R_{TOA}) with a consequent reduction in the retrieved CF. The reduction in CF will further reduce the retrieved CP if the amount of AMF in the cloudy portion of the pixel (AMF_{cl}) is smaller than the AMF in the clear-sky portion (AMF_{cr}); whereas it has an opposite effect when the AMF_{cl} exceeds the AMF_{cr}. In retrieving NO₂, the increased Rs also enhances the AMF of NO₂.

Title Page

Abstract

Introduction

Conclusions

References

Tables

Figures

◀

▶

Back

Close

Full Screen / Esc

Printer-friendly Version

Interactive Discussion



Cases 3–4 assume blue-sky albedo and black-sky albedo, respectively, derived from the MODIS BRDF data. The black-sky albedo accounts for the incident solar radiation reflected by isotropic surface, while the blue-sky albedo accounts for both direct and diffuse radiation reaching the ground. The relative contributions of direct and diffuse radiation are determined using the LUT developed by Lucht et al. (2000). The resulting blue-sky albedo and black-sky albedo differ insignificantly from the MODIS BRF with a difference within ± 0.01 for all pixels. They result in cloud properties and NO₂ columns very close to our reference retrieval (Fig. 6d–i).

Case 5 adopts the monthly As climatology based on the OMI measurements over 2005–2009 (OMLER v3; 0.5° lon \times 0.5° lat). During our retrieval process, the albedo for a given day is interpolated from the closest two months. The resulting albedo is larger than the MODIS BRF for 78 % of the pixels with an average difference of 0.023. On average, it results in lower CFs and CRFs by 0.01 and 0.04, respectively (Fig. 6d and f). It enhances the AMFs of NO₂ by 7 % averaged over the pixels with a consequent negative effect on the retrieved NO₂ columns by 7 % on average (Fig. 6h and i). Pixel by pixel, the reduction in NO₂ columns can reach 45 %.

Case 6 uses the same albedo as DOMINO-2. The resulting changes in CF are within ± 0.05 for all pixels (within ± 0.1 for CRF). Overall, adopting the albedo from DOMINO-2 has a small impact on the AMF and VCD of NO₂ with a negligible NMD relative to Case 0 (Fig. 6h and i). The small difference is due to the changes in clouds compensating for the effects of the perturbed Rs, despite the large changes in Rs (Fig. 2a). Had the CF and CP not been modified in accordance to the perturbed Rs, the influence of Rs would have been larger.

5.2 Effects of the vertical profile of NO₂

The assumed vertical profile of NO₂ affects the NO₂ retrieval because the layer AMFs decline with height in the troposphere (e.g., Fig. 3a). For example, assuming NO₂ to be closer to the ground reduces the AMF with a positive effect on the retrieved NO₂ column. The cloud retrieval is not affected. Cases 7–11 change the vertical profile of

[Title Page](#)[Abstract](#)[Introduction](#)[Conclusions](#)[References](#)[Tables](#)[Figures](#)[|◀](#)[▶|](#)[◀](#)[▶|](#)[Back](#)[Close](#)[Full Screen / Esc](#)[Printer-friendly Version](#)[Interactive Discussion](#)

Retrieving tropospheric nitrogen dioxide over China

J.-T. Lin et al.

[Title Page](#)[Abstract](#)[Introduction](#)[Conclusions](#)[References](#)[Tables](#)[Figures](#)[|◀](#)[▶|](#)[◀](#)[▶](#)[Back](#)[Close](#)[Full Screen / Esc](#)[Printer-friendly Version](#)[Interactive Discussion](#)

5.3 Effects of aerosol optics

Aerosol optics affects the retrievals of cloud properties and NO₂ columns (Boersma et al., 2004; Leitão et al., 2010; Boersma et al., 2011). In retrieving the cloud information, aerosol scattering enhances the R_{TOA} , thus reducing the CF (Fig. 8). It increases the AMF of O₂-O₂ with a negative effect on the CP. Aerosol scattering also enhances the AMF of NO₂ when aerosols are collocated with or located below NO₂. Aerosol absorption has opposite effects by enhancing the CF and CP and reducing the AMF of NO₂. Furthermore, the height of aerosols is important for their influences on the R_{TOA} and on the AMFs of O₂-O₂ and NO₂. In this section, we first evaluate the effects 5 of aerosol scattering and absorption in retrieving clouds and NO₂ based on the simulated vertical distribution of aerosols. We then analyze the influences of the vertical 10 distribution of aerosols, keeping the AOD and SSA unchanged.

5.4 Effects of aerosol scattering and absorption based on the simulated vertical distribution of aerosols

15 Compared to Case 0, Case 12 does not include the optical effects of aerosols, as is done in the retrieval processes of OMCLDO2 and DOMINO-2. It thus enhances the CFs and CRFs for all of the 127 pixels (Fig. 9a). A modest correlation is found ($R^2 = 0.66$) between the amounts of decremented AOD and the amounts of incremented CF; and there is large scattering in the increments of CF for pixels with AOD of 1.5 or more. 20 The CP is also affected, but the changes in CP do not correlate with the amounts of decremented AOD ($R^2 = 0.10$). Case 12 produces CF and CRF that are consistent with DOMINO-2 (OMCLDO2) with small differences averaged over the 127 pixels; the differences are much larger for individual pixels (within 0.06 for CF and within 0.27 for CRF; see Fig. 10) as a result of their differences in Rs, pressure and temperature 25 profiles, and other aerosol characteristics (e.g., SSA, vertical distribution; Boersma et al., 2011). The CP produced by Case 12 is larger than DOMINO-2 (OMCLDO2)

[Title Page](#)[Abstract](#)[Introduction](#)[Conclusions](#)[References](#)[Tables](#)[Figures](#)[|◀](#)[▶|](#)[Back](#)[Close](#)[Full Screen / Esc](#)[Printer-friendly Version](#)[Interactive Discussion](#)

Retrieving tropospheric nitrogen dioxide over China

J.-T. Lin et al.

[Title Page](#)[Abstract](#)[Introduction](#)[Conclusions](#)[References](#)[Tables](#)[Figures](#)[◀](#)[▶](#)[Back](#)[Close](#)[Full Screen / Esc](#)[Printer-friendly Version](#)[Interactive Discussion](#)

(Fig. 10), and the difference is not caused by the different Ps data used according to our test cloud retrieval adopting the Ps data from OMCLDO2.

The exclusion of aerosols results in mixed changes in the AMF of NO₂. Compared to Case 0, Case 12 enhances the AMFs by 0–0.8 for 91 pixels with negative effects by 0–0.4 for the other 36 pixels. No correlation is found between the amounts of AOD omitted and the amounts of AMF changed ($R^2 = 0.03$). This has an important impact on the retrieved NO₂ columns. As shown in Fig. 11a, Case 12 can result in NO₂ columns either larger or smaller than Case 0. There is notable scattering in the magnitude and signs of the differences between the two cases ($R^2 = 0.15$ between the decremented AOD and the NO₂ change), particularly when the AOD is high. Of the 44 pixels with AOD of 0.8 or more, Case 12 results in larger NO₂ columns by 0–50 molec. cm⁻² $\times 10^{15}$ molec. cm⁻² for 18 pixels with negative effects by 0–20 molec. cm⁻² $\times 10^{15}$ molec. cm⁻² for the other 26 pixels. Overall, although the NMD relative to Case 0 is only 2 % for NO₂ columns across the 127 pixels, the NMAD reaches a relatively high value of 20 % (Fig. 6i).

Case 13 assumes no aerosol absorption, thus reducing the amounts of CF and CRF as compared to Case 0 (Fig. 9c). However, the reductions in CF and CRF do not correlate strongly with the amounts of absorption (AAOD) neglected ($R^2 = 0.37$ for CF and 0.41 for CRF), particularly when the AAOD is high. There is a large variation in the decremented CP relative to the amounts of AAOD neglected ($R^2 = 0.27$). Furthermore, Case 13 does not lead to universally increases nor decreases in the AMF and VCD of NO₂; overall, an increasing amount of AAOD neglected results in an increased AMF and a decreased VCD with R^2 of 0.34 and 0.40, respectively (Fig. 11c). For Case 13, the NMD and NMAD for NO₂ columns relative to Case 0 are –10 % and 12 %, respectively.

Emissions of black carbon in China have been under debate recently (Fu et al., 2012; Wang et al., 2013). The top-down constraint by Fu et al. (2012) suggested Chinese black carbon emissions to be underestimated by about 60 % by the INTEX-B inventory. In contrast, Wang et al. (2013) suggested consistent magnitudes of emissions between their top-down calculation and the INTEX-B data, after filtering out high pollution

Title Page

Abstract

Introduction

Conclusions

References

Tables

Figures

◀

▶

◀

▶

Back

Close

Full Screen / Esc

Printer-friendly Version

Interactive Discussion



plumes and large precipitation events (for which cases they determined that the CTM was limited by model resolution and wet deposition errors). In light of these studies, we conducted another test (Case 14) by doubling the amount of aerosol absorption, recognizing that black carbon emissions and thus aerosol absorption could have been underestimated by Case 0. The resulting changes in clouds and NO₂ columns are consistent with Case 13 but with opposite signs (Fig. 6d–i).

We further evaluate the sole effect of aerosol scattering by contrasting Case 12 (neglecting both scattering and absorption) to Case 13 (neglecting absorption). As shown in Fig. 9b, the incremented CFs and CRFs in Case 12 relative to Case 13 correlate strongly with the amounts of decremented scattering (ASOD) with R^2 of 0.84 for CF and of 0.82 for CRF. This is consistent with the analysis by Boersma et al. (2011) for the Southeastern US. The changes in CP do not correlate with the amounts of ASOD omitted ($R^2 = 0.12$). Figure 11b further shows that neglecting aerosol scattering can either increase or decrease the AMF and VCD of NO₂ with no obvious dependence on the amounts of ASOD neglected. On average, Case 12 differs from Case 13 by 13 % for NO₂ columns with a mean absolute difference by 30 %.

5.5 Effects of the vertical distribution of aerosols under given AOD and SSA

The MAX-DOAS sites are located in the urban or suburban areas; therefore aerosols and NO₂ are dominated by anthropogenic sources and are collocated in the lower troposphere. Figure 3c illustrates the vertical distributions of the EC and SSA of aerosols for a pixel on 28 December 2008 assumed in Case 0. Cases 15–17 test the influences of the vertical distribution of aerosols on the retrievals of clouds and NO₂, without altering the AOD and SSA (Table 4).

Case 15 assumes constant EC and SSA of aerosols throughout the troposphere, as an extreme case for the vertical distribution of aerosols. It enhances both scattering and absorption of aerosols at high altitudes, thus reducing the AMF of O₂-O₂ that is compensated for by an increase in CP. It increases the CFs for 71 % of the pixels, in compensating for the effect of enhanced aerosol absorption on the R_{TOA} . Putting more

Title Page	
Abstract	Introduction
Conclusions	References
Tables	Figures
◀	▶
◀	▶
Back	Close
Full Screen / Esc	
Printer-friendly Version	
Interactive Discussion	



aerosols above NO_2 also reduces the AMF of NO_2 . Compared to Case 0, Case 15 suggests larger NO_2 columns for 92 % of the pixels with a NMD of 18 % and a NMAD of 30 % (Fig. 6i).

Case 16 puts all aerosols at the PBL top, thus lowering the contributions of $\text{O}_2\text{-O}_2$ and NO_2 in the PBL. It increases the CFs for half of the pixels with negative effects for one third of the pixels. The resulting AMFs of NO_2 are lower than Case 0 for 74 % of the pixels and do not correlate strongly with Case 0 ($R^2 = 0.50$; Fig. 7). Across the pixels, the NMD for NO_2 columns is only about 8 % but the NMAD reaches 23 % (Fig. 6i).

As another extreme experiment, Case 17 assumes aerosols to be concentrated at the tropopause. It enhances the CFs for two thirds of the pixels, because the effect of enhanced aerosol absorption on the R_{TOA} overcompensates for the effect of enhanced aerosol scattering. It reduces the AMFs of NO_2 for 61 % of the pixels; and the changes in AMF correlate poorly with the amounts of AOD. Overall, Case 17 correlates weakly with Case 0 for the AMF ($R^2 = 0.17$) and VCD ($R^2 = 0.46$) of NO_2 (Fig. 7). Its NMD and NMAD for NO_2 columns relative to Case 0 amount to 29 % and 47 %, respectively (Fig. 6i).

5.6 Discussions

Despite the large differences in ancillary parameters and thus AMFs, Cases 0–17 produce NO_2 columns with modest to high correlation to the MAX-DOAS measurements.

As shown in Fig. 12, the R^2 ranges from 0.69 to 0.96 for the 30 daily data complying with the spatial constraints (pixel-center distance $\leq 25 \text{ km}$; VZA $\leq 30^\circ$). In particular, mimicking the inconsistent treatments of Ps and clouds between DOMINO-2 and OM-CLDO2 (Case 1) results in R^2 of 0.85 and slope of 1.06. Assuming an arbitrarily large vertical gradient of NO_2 (Case 11) leads to R^2 of 0.93 with slope of 1.27. Confining aerosols to the tropopause (Case 17) results in R^2 of 0.69 and slope of 0.77. This is because most of the day-to-day variability in the MAX-DOAS data can be explained by the SCDs retrieved from OMI and the geometry of the light path (i.e., $R^2 = 0.87$ be-

Title Page	
Abstract	Introduction
Conclusions	References
Tables	Figures
◀	▶
◀	▶
Back	Close
Full Screen / Esc	
Printer-friendly Version	
Interactive Discussion	

tween MAX-DOAS VCD and OMI gVCD). More MAX-DOAS measurements located in different representative regions (both polluted and clean areas) are needed to further identify the effects of individual ancillary parameters in retrieving NO₂ columns from OMI. Also, MAX-DOAS measurements should be complemented by regular measurements of the NO₂ vertical distribution such as the NO₂ sondes demonstrated by Sluis et al. (2010).

With the optimized treatment of ancillary parameters, our reference retrieval (Case 0) suggests NO₂ columns to be about half of the MAX-DOAS measurements. Adopting the vertical profiles of NO₂ from the MAX-DOAS retrieval (Case 7) results in NO₂ columns that are still lower than MAX-DOAS by 36 %. Part of the difference may lie in the inevitable spatial inconsistency between the ground- and space-based remote sensing: the MAX-DOAS sensors always face north and typically sample a horizontal distance of a few kilometers, while an OMI pixel represents an area of 13 km² × 24 km² or larger. Brinksma et al. (2008) showed that changing the azimuth angle of the MAX-DOAS sensor can result in differences by a factor of 10–350 % (by 50 % on average) in the retrieved NO₂ in Cabauw, the Netherlands due to the influences of local sources and/or sinks (see their Fig. 6). The influence of horizontal inhomogeneity in NO₂ was suggested to be about 10–30 % for MAX-DOAS measurements taken at the Chinese Meteorological Administration in urban Beijing (Ma et al., 2013) and about 10–15 % for Tai'An, Mangshan, and Rudong (Irie et al., 2012) in East China (see Fig. 1 for locations of these sites). As shown in Fig. 1, Xianghe, Tai'An, Mangshan and Rudong are less polluted than Beijing with weaker horizontal inhomogeneity of NO₂. By comparison, about 77 % of the 127 OMI pixels analyzed here are located near Beijing IAP with larger NO₂ gradient. Irie et al. (2012) also showed that the vicinity of the polluted Yokosuka site undergoes larger horizontal variability of NO₂. Irie et al. (2012) analyzed the sensitivity of the DOMINO-2–MAX-DOAS consistency to the pixel-center distance with no restrictions on the VZA. Figure 5 shows that a stricter VZA constraint enhances the sensitivity of the slope to the distance constraint. The effect of horizontal inhomogeneity is also in line with the pixel-specific comparison in Fig. 4b that shows notable scatter-



Title Page	
Abstract	Introduction
Conclusions	References
Tables	Figures
◀	▶
◀	▶
Back	Close
Full Screen / Esc	
Printer-friendly Version	
Interactive Discussion	



ing in the OMI data in a given day corresponding to a MAX-DOAS site. Overall, we tentatively estimate the effect of horizontal inhomogeneity (and spatial inconsistency between space- and ground-based measurements) to be 20–30 % for the 127 OMI pixels analyzed here. This estimate is preliminary since previous studies suggested
5 the spatial inhomogeneity to be strongly location-, time- and meteorology-dependent (Brinksma et al., 2008; Irie et al., 2012; Ma et al., 2013). The differences between our reference retrieval and MAX-DOAS data may also be contributed by errors in MAX-DOAS measurements (by 11–14%; Irie et al., 2012; Hendrick et al., 2013). Also, our retrieval process may still be affected by residual uncertainties associated with SSA of
10 aerosols (by 10 % based on Cases 12–14), vertical distribution of aerosols (by 10 % based on Case 16), and vertical profile of NO₂ (by 10–20 % based on Cases 7–8). These uncertainties may complement or compensate for each other.

6 Conclusions

Using LIDORT v3.6, we developed an improved AMF formulation (AMFv6) to evaluate
15 the effects of aerosols, surface reflectance anisotropy, and vertical profile of NO₂ in retrieving the tropospheric NO₂ columns from OMI. As a reference case, we retrieved the vertical columns by calculating the AMFs of NO₂ independently and adopting the tropospheric SCDs from the widely used DOMINO-2 product. We retrieved the cloud properties prior to the retrieval of NO₂ using consistent ancillary parameters including
20 but not limited to surface pressure, surface reflectance, and aerosols. We accounted for surface reflectance anisotropy. Also, we explicitly accounted for the effect of aerosols on the solar radiation during the retrieval process. We compared DOMINO-2 to our NO₂ retrieval, using as reference the ground-based MAX-DOAS measurements at three urban/suburban sites in East China and focusing on the 127 OMI pixels (in 30 days)
25 complying with our spatial constraints (pixel-center distance \leq 25 km; VZA \leq 30°). We then perturbed the individual ancillary parameters to evaluate their influences on the retrieved cloud properties and NO₂ columns.

Retrieving tropospheric nitrogen dioxide over China

J.-T. Lin et al.

The magnitude of NO₂ columns retrieved by DOMINO-2 appears consistent with the MAX-DOAS measurements. However, this is due mainly to the overestimate of surface pressure and the inconsistent treatments of surface pressure between DOMINO-2 and OMCLDO2 (from which DOMINO-2 takes the cloud data). The retrieval processes of DOMINO-2 and OMCLDO2 do not include the aerosol optics. The resulting cloud pressure, cloud fraction and cloud radiance fraction are subject to aerosol interferences, an important issue for China concerning its high aerosol concentrations.

Our reference retrieval for NO₂ and clouds adopts the surface BRDF data from MODIS and the vertical profiles of aerosols and NO₂ from the nested GEOS-Chem simulations. The modeled aerosol optics is further constrained by AOD measurements from AERONET, MAX-DOAS or MODIS. By explicitly accounting for aerosol optics, our retrieval results in cloud properties with reduced aerosol interferences, thus increasing the number of valid OMI pixels with low cloud coverage (CRF \leq 50 %) by about 25 % for the pixels investigated here. Our retrieved NO₂ columns highly correlate with the MAX-DOAS data ($R^2 = 0.96$ for the 30 selected days) while the magnitude is about half of the latter. The difference is due to the inevitable spatial inconsistency between the ground- and space-based remote sensing (by 20–30 %), uncertainties in MAX-DOAS measurements (by 11–14 %), and residual errors in our OMI NO₂ retrieval associated with aerosols (SSA and vertical distribution; by 10 % each) and vertical shape of NO₂ (by 10–20 %). The estimate for the effect of spatial inconsistency is preliminary since the spatial inhomogeneity of NO₂ strongly depends on the locations, time and meteorological conditions (Brinksma et al., 2008; Irie et al., 2012; Ma et al., 2013).

In retrieving the cloud information, the changes in cloud pressure in response to the inclusion/exclusion of aerosol scattering do not correlate with the amounts of aerosol scattering ($R^2 = 0.12$), although the changes in cloud fraction are highly correlated to aerosol scattering ($R^2 = 0.84$). The changes in both cloud fraction and cloud pressure due to the inclusion/exclusion of aerosol absorption do not correlate strongly to the amounts of aerosol absorption ($R^2 < 0.42$). Furthermore, the inclusion or exclusion of aerosol optics results in very different AMFs and VCDs of tropospheric NO₂ particular

21229



when the AOD is large. The absolute difference in NO₂ columns amounts to 20 % for the 127 pixels examined. This reveals a difficulty in using DOMINO-2 (and other current satellite NO₂ products) for individual pixels or days for further applications such as emission inversion due to lack of an explicit treatment of aerosols. Meanwhile, we
5 find the difference is only 2 % for the 127-pixel mean NO₂ column with or without explicitly accounting for the aerosol optics in the retrieval process, likely suggesting that the effect of aerosols may be canceled out by spatiotemporal averaging. Given the limited number of locations examined here, further studies on a larger domain (e.g., East China) are required to fully reveal the effects of aerosols on the satellite-retrieved
10 NO₂ columns. We are currently in the process of doing such analysis (J.-T. Lin et al., Improved retrieval of the tropospheric NO₂ seasonality from the Ozone Monitoring Instrument, 2013).

We used a variety of surface reflectance datasets to evaluate the resulting impacts on the retrieved cloud information and NO₂ columns. Adopting the MODIS blue-sky
15 albedo or black-sky albedo, in place of the treatment of surface BRDF, has a negligible effect on the retrieved clouds and NO₂ columns for the 127 pixels examined. Employing the OMLER v3 surface albedo data reduces the NO₂ columns by 7 % on average with larger effects for individual pixels (−45 %–7 %). Adopting the albedo data used by DOMINO-2 (OMLER v1) has a small effect on the retrieved NO₂ columns on average,
20 due to the compensation by the corresponding adjustment in clouds.

Assumptions on the vertical profiles of aerosols and NO₂ also have large influences in retrieving clouds and/or NO₂ columns from OMI. Adopting the NO₂ profiles derived
25 from the MAX-DOAS measurements enhances the retrieved NO₂ columns by 20 % averaged over the 127 pixels. Using the profiles simulated by TM4 increases the NO₂ columns by 10 % on average. Assuming an exponential decrease of NO₂ from the surface to 3 km (with a scale height of 0.25 km) enhances the retrieved NO₂ columns by 82 % on average, bringing the mean value closer to the MAX-DOAS result.

We find that various assumptions on aerosols, surface reflectance and the vertical profile of NO₂ during the retrieval process result in NO₂ columns correlated at least

[Title Page](#)

[Abstract](#)

[Introduction](#)

[Conclusions](#)

[References](#)

[Tables](#)

[Figures](#)

◀

▶

◀

▶

[Back](#)

[Close](#)

[Full Screen / Esc](#)

[Printer-friendly Version](#)

[Interactive Discussion](#)



modestly ($R^2 \geq 0.69$) with the MAX-DOAS data. This is likely a result of the limited MAX-DOAS measurements concentrating in the urban/suburban areas so that the variability of NO_2 are dominated by the alternations of clean and polluted days and that the differences in the calculated AMFs have a secondary effect. More MAX-DOAS measurements, together with NO_2 sondes, in more representative regions (both polluted and clean areas) will help separate the effects of individual ancillary assumptions on the retrieval of NO_2 columns.

As a concluding remark, the effects of aerosols and surface reflectance anisotropy found here also have important implications for the retrievals of other species (sulfur dioxide, formaldehyde, glyoxal, etc.) from OMI and/or other UV/VIS backscatter instruments. We recommend that aerosols and surface reflectance anisotropy be explicitly accounted for in future satellite retrievals, especially when a near-real-time retrieval (fast computation) is not required so that these factors can be well characterized for individual pixels in the retrieval process without the use of a look-up table. In addition, we suggest using high-resolution vertical profiles of tracers in the retrieval process to better characterize their spatial inhomogeneity.

Appendix A

We used the nested GEOS-Chem model for Asia (v8–3–2; Chen et al., 2009), at $0.667^\circ \text{lon} \times 0.5^\circ \text{lat}$ with 47 layers, to simulate vertical profiles of NO_2 and aerosol optical properties. The model is driven by the GEOS-5 assimilated meteorological fields from the NASA Global Modeling and Assimilation Office (GMAO). It is run with the full $\text{O}_x\text{-NO}_x\text{-VOC-CO-HO}_x$ gaseous chemistry with online aerosol calculations. Vertical mixing in the planetary boundary layer is simulated by a non-local parameterization scheme (Lin and McElroy, 2010). The simulation of convection is based on a modified Relaxed Arakawa-Schubert scheme (Rienecker et al., 2008). Asian anthropogenic emissions are taken from the INTEX-B dataset (Zhang et al., 2009). Lightning emis-

Title Page	
Abstract	Introduction
Conclusions	References
Tables	Figures
◀	▶
◀	▶
Back	Close
Full Screen / Esc	
Printer-friendly Version	
Interactive Discussion	



Title Page

Abstract

Introduction

Conclusions

References

Tables

Figures

◀

▶

◀

▶

Back

Close

Full Screen / Esc

Printer-friendly Version

Interactive Discussion



sions of NO_x follow Price et al. (1997) with a local correction based on the OTD/LIS satellite measurements (Sauvage et al., 2007; Murray et al., 2012), and are distributed vertically with a backward “C-shape” profile (Ott et al., 2010). Soil emissions of NO_x follow Yienger and Levy (1995) and Wang et al. (1998). More model descriptions can 5 be found in Lin (2012) and Lin et al. (2012).

For aerosols, GEOS-Chem simulate sulfates, nitrates, ammoniums (Park et al., 2004, 2006), black carbon, organic carbon (Park et al., 2003, 2006), dust (Fairlie et al., 2010), and sea salts (Alexander et al., 2005; Jaeglé et al., 2011). The general structure of 10 the aerosol simulations is presented by Park et al. (2004, 2006). The sulfate-nitrate-ammonium aerosols are simulated by the thermodynamical equilibrium scheme of ISOROPIA-II (Fountoukis and Nenes, 2007). Emissions of mineral dusts adopt the DEAD scheme (Zender et al., 2003). Aerosol microphysical properties follow Drury et al. (2010), including dry size distributions, hygroscopic growth factors, and refractive 15 indices.

15 **Acknowledgements.** This research is supported by the National Natural Science Foundation of China, grant 41005078, 41175127 and 41175030. We thank Huan Yu and Dominik Brunner for discussions on the radiative transfer modeling. We acknowledge the free use of NO₂ and cloud products from www.temis.nl, surface elevation data from USGS, MODIS aerosol and surface reflectance data from NASA, and AOD measurements from AERONET. MAX-DOAS measurements in Beijing and Xianghe have been supported through the EU FP7 project NORS and by 20 the Belgian Science Policy (IBBAC contract BL/35/C60, and AGACC project, grant SD/CS/07A).

References

- 25 Acarreta, J. R., De Haan, J. F., and Stammes, P.: Cloud pressure retrieval using the O₂-O₂ absorption band at 477 nm, *J. Geophys. Res.-Atmos.*, 109, D05204, doi:10.1029/2003jd003915, 2004.
Alexander, B., Park, R. J., Jacob, D. J., Li, Q. B., Yantosca, R. M., Savarino, J., Lee, C. C. W., and Thiemens, M. H.: Sulfate formation in sea-salt aerosols: constraints from oxygen isotopes, *J. Geophys. Res.-Atmos.*, 110, D10307, doi:10.1029/2004jd005659, 2005.

Anderson, G. P., Clough, S. A., Kneizys, F. X., Chetwynd, J. H., and Shettle, E. P.: AFGL Atmospheric Constituent Profiles, Air Force Geophys. Lab., Tech. Rep. AFGL-TR-86-0110, Hanscom AFB, Mass., 1986.

Beirle, S., Boersma, K. F., Platt, U., Lawrence, M. G., and Wagner, T.: Megacity emissions and lifetimes of nitrogen oxides probed from space, *Science*, 333, 1737–1739, doi:10.1126/science.1207824, 2011.

Boersma, K. F., Eskes, H. J., and Brinksma, E. J.: Error analysis for tropospheric NO₂ retrieval from space, *J. Geophys. Res.*, 109, D04311, doi:10.1029/2003JD003962, 2004.

Boersma, K. F., Eskes, H. J., Veefkind, J. P., Brinksma, E. J., van der A, R. J., Sneep, M., van den Oord, G. H. J., Levelt, P. F., Stammes, P., Gleason, J. F., and Bucsela, E. J.: Near-real time retrieval of tropospheric NO₂ from OMI, *Atmos. Chem. Phys.*, 7, 2103–2118, doi:10.5194/acp-7-2103-2007, 2007.

Boersma, K. F., Eskes, H. J., Dirksen, R. J., van der A, R. J., Veefkind, J. P., Stammes, P., Huijnen, V., Kleipool, Q. L., Sneep, M., Claas, J., Leitão, J., Richter, A., Zhou, Y., and Brunner, D.: An improved tropospheric NO₂ column retrieval algorithm for the Ozone Monitoring Instrument, *Atmos. Meas. Tech.*, 4, 1905–1928, doi:10.5194/amt-4-1905-2011, 2011.

Brinksma, E. J., Pinardi, G., Volten, H., Braak, R., Richter, A., Schonhardt, A., van Roozendael, M., Fayt, C., Hermans, C., Dirksen, R. J., Vlemmix, T., Berkhouw, A. J. C., Swart, D. P. J., Oetjen, H., Wittrock, F., Wagner, T., Ibrahim, O. W., de Leeuw, G., Moerman, M., Curier, R. L., Celarier, E. A., Cede, A., Knap, W. H., Veefkind, J. P., Eskes, H. J., Allaart, M., Rothe, R., Piters, A. J. M., and Levelt, P. F.: The 2005 and 2006 DANDELIONS NO₂ and aerosol inter-comparison campaigns, *J. Geophys. Res.-Atmos.*, 113, D16S46, doi:10.1029/2007jd008808, 2008.

Bucsela, E. J., Perring, A. E., Cohen, R. C., Boersma, K. F., Celarier, E. A., Gleason, J. F., Wenig, M. O., Bertram, T. H., Wooldridge, P. J., Dirksen, R., and Veefkind, J. P.: Comparison of tropospheric NO₂ from in situ aircraft measurements with near-real-time and standard product data from OMI, *J. Geophys. Res.-Atmos.*, 113, D16s31, doi:10.1029/2007jd008838, 2008.

Bucsela, E. J., Krotkov, N. A., Celarier, E. A., Lamsal, L. N., Swartz, W. H., Bhartia, P. K., Boersma, K. F., Veefkind, J. P., Gleason, J. F., and Pickering, K. E.: A new stratospheric and tropospheric NO₂ retrieval algorithm for nadir-viewing satellite instruments: applications to OMI, *Atmos. Meas. Tech. Discuss.*, 6, 1361–1407, doi:10.5194/amtd-6-1361-2013, 2013.

Retrieving tropospheric nitrogen dioxide over China

J.-T. Lin et al.

[Title Page](#)

[Abstract](#)

[Introduction](#)

[Conclusions](#)

[References](#)

[Tables](#)

[Figures](#)

◀

▶

◀

▶

[Back](#)

[Close](#)

[Full Screen / Esc](#)

[Printer-friendly Version](#)

[Interactive Discussion](#)



- Castellanos, P. and Boersma, K. F.: Reductions in nitrogen oxides over Europe driven by environmental policy and economic recession, *Sci. Rep.*, 2, 265, doi:10.1038/srep00265, 2012.
- Chen, D., Wang, Y., McElroy, M. B., He, K., Yantosca, R. M., and Le Sager, P.: Regional CO pollution and export in China simulated by the high-resolution nested-grid GEOS-Chem model, *Atmos. Chem. Phys.*, 9, 3825–3839, doi:10.5194/acp-9-3825-2009, 2009.
- Cheng, Z., Jiang, J. K., Fajardo, O., Wang, S. X., and Hao, J. M.: Characteristics and health impacts of particulate matter pollution in China (2001–2011), *Atmos. Environ.*, 65, 186–194, doi:10.1016/j.atmosenv.2012.10.022, 2013.
- Clément, K., Van Roozendael, M., Fayt, C., Hendrick, F., Hermans, C., Pinardi, G., Spurr, R., Wang, P., and De Mazière, M.: Multiple wavelength retrieval of tropospheric aerosol optical properties from MAXDOAS measurements in Beijing, *Atmos. Meas. Tech.*, 3, 863–878, doi:10.5194/amt-3-863-2010, 2010.
- Dieudonné, E., Ravetta, F., Pelon, J., Goutail, F., and Pommereau, J.-P.: Linking NO₂ surface concentration and integrated content in the urban developed atmospheric boundary layer, *Geophys. Res. Lett.*, 40, 1247–1251, doi:10.1002/grl.50242, 2013.
- Drury, E., Jacob, D. J., Spurr, R. J. D., Wang, J., Shinozuka, Y., Anderson, B. E., Clarke, A. D., Dibb, J., McNaughton, C., and Weber, R.: Synthesis of satellite (MODIS), aircraft (ICARTT), and surface (IMPROVE, EPA-AQS, AERONET) aerosol observations over eastern North America to improve MODIS aerosol retrievals and constrain surface aerosol concentrations and sources, *J. Geophys. Res.-Atmos.*, 115, D14204, doi:10.1029/2009jd012629, 2010.
- Fairlie, T. D., Jacob, D. J., Dibb, J. E., Alexander, B., Avery, M. A., van Donkelaar, A., and Zhang, L.: Impact of mineral dust on nitrate, sulfate, and ozone in transpacific Asian pollution plumes, *Atmos. Chem. Phys.*, 10, 3999–4012, doi:10.5194/acp-10-3999-2010, 2010.
- Ford, B. and Heald, C. L.: An A-train and model perspective on the vertical distribution of aerosols and CO in the Northern Hemisphere, *J. Geophys. Res.-Atmos.*, 117, D06211, doi:10.1029/2011jd016977, 2012.
- Fountoukis, C. and Nenes, A.: ISORROPIA II: a computationally efficient thermodynamic equilibrium model for K₊–Ca₂₊–Mg₂₊–NH₄₊–Na₊–SO₄₂₋–NO₃₋–Cl₋–H₂O aerosols, *Atmos. Chem. Phys.*, 7, 4639–4659, doi:10.5194/acp-7-4639-2007, 2007.
- Fu, T.-M., Cao, J. J., Zhang, X. Y., Lee, S. C., Zhang, Q., Han, Y. M., Qu, W. J., Han, Z., Zhang, R., Wang, Y. X., Chen, D., and Henze, D. K.: Carbonaceous aerosols in China: top-down constraints on primary sources and estimation of secondary contribution, *Atmos. Chem. Phys.*, 12, 2725–2746, doi:10.5194/acp-12-2725-2012, 2012.

Retrieving
tropospheric nitrogen
dioxide over China

J.-T. Lin et al.

Title Page

Abstract

Introduction

Conclusions

References

Tables

Figures

|◀

▶|

Back

Close

Full Screen / Esc

Printer-friendly Version

Interactive Discussion



Hains, J. C., Boersma, K. F., Kroon, M., Dirksen, R. J., Cohen, R. C., Perring, A. E., Bucsela, E., Volten, H., Swart, D. P. J., Richter, A., Wittrock, F., Schoenhardt, A., Wagner, T., Ibrahim, O. W., van Roozendael, M., Pinardi, G., Gleason, J. F., Veefkind, J. P., and Levelt, P.: Testing and improving OMI DOMINO tropospheric NO₂ using observations from the DANDELIONS and INTEX-B validation campaigns, *J. Geophys. Res.-Atmos.*, 115, D05301, doi:10.1029/2009jd012399, 2010.

Hendrick, F., Müller, J.-F., Clémér, K., Mazière, M. D., Fayt, C., Hermans, C., Stavrakou, T., Vlemmix, T., Wang, P., and Roozendael, M. V.: Four years of ground-based MAX-DOAS observations of HONO and NO₂ in the Beijing area, submitted to *Atmos. Chem. Phys.*, 2013.

Herman, J. R., Celarier, E., and Larko, D.: UV 380 nm reflectivity of the Earth's surface, clouds and aerosols, *J. Geophys. Res.-Atmos.*, 106, 5335–5351, doi:10.1029/2000jd900584, 2001.

Hudman, R. C., Russell, A. R., Valin, L. C., and Cohen, R. C.: Interannual variability in soil nitric oxide emissions over the United States as viewed from space, *Atmos. Chem. Phys.*, 10, 9943–9952, doi:10.5194/acp-10-9943-2010, 2010.

Hyer, E. J., Reid, J. S., and Zhang, J.: An over-land aerosol optical depth data set for data assimilation by filtering, correction, and aggregation of MODIS Collection 5 optical depth retrievals, *Atmos. Meas. Tech.*, 4, 379–408, doi:10.5194/amt-4-379-2011, 2011.

Irie, H., Kanaya, Y., Akimoto, H., Tanimoto, H., Wang, Z., Gleason, J. F., and Bucsela, E. J.: Validation of OMI tropospheric NO₂ column data using MAX-DOAS measurements deep inside the North China Plain in June 2006: Mount Tai Experiment 2006, *Atmos. Chem. Phys.*, 8, 6577–6586, doi:10.5194/acp-8-6577-2008, 2008.

Irie, H., Takashima, H., Kanaya, Y., Boersma, K. F., Gast, L., Wittrock, F., Brunner, D., Zhou, Y., and Van Roozendael, M.: Eight-component retrievals from ground-based MAX-DOAS observations, *Atmos. Meas. Tech.*, 4, 1027–1044, doi:10.5194/amt-4-1027-2011, 2011.

Irie, H., Boersma, K. F., Kanaya, Y., Takashima, H., Pan, X., and Wang, Z. F.: Quantitative bias estimates for tropospheric NO₂ columns retrieved from SCIAMACHY, OMI, and GOME-2 using a common standard for East Asia, *Atmos. Meas. Tech.*, 5, 2403–2411, doi:10.5194/amt-5-2403-2012, 2012.

Jaeglé, L., Quinn, P. K., Bates, T. S., Alexander, B., and Lin, J.-T.: Global distribution of sea salt aerosols: new constraints from in situ and remote sensing observations, *Atmos. Chem. Phys.*, 11, 3137–3157, doi:10.5194/acp-11-3137-2011, 2011.

Retrieving tropospheric nitrogen dioxide over China

J.-T. Lin et al.

[Title Page](#)

[Abstract](#)

[Introduction](#)

[Conclusions](#)

[References](#)

[Tables](#)

[Figures](#)

◀

▶

◀

▶

[Back](#)

[Close](#)

[Full Screen / Esc](#)

[Printer-friendly Version](#)

[Interactive Discussion](#)



Retrieving
tropospheric nitrogen
dioxide over China

J.-T. Lin et al.

Title Page

Abstract

Introduction

Conclusions

References

Tables

Figures

◀

▶

◀

▶

Back Close

Full Screen / Esc

Printer-friendly Version

Interactive Discussion



- Kleipool, Q. L., Dobber, M. R., de Haan, J. F., and Levelt, P. F.: Earth surface reflectance climatology from 3 years of OMI data, *J. Geophys. Res.-Atmos.*, 113, D18308, doi:10.1029/2008jd010290, 2008.
- Lamsal, L. N., Martin, R. V., van Donkelaar, A., Steinbacher, M., Celarier, E. A., Bucsela, E.,
5 Dunlea, E. J., and Pinto, J. P.: Ground-level nitrogen dioxide concentrations inferred from the satellite-borne Ozone Monitoring Instrument, *J. Geophys. Res.-Atmos.*, 113, D16308, doi:10.1029/2007jd009235, 2008.
- Lamsal, L. N., Martin, R. V., Padmanabhan, A., van Donkelaar, A., Zhang, Q., Sioris, C. E.,
10 Chance, K., Kurosu, T. P., and Newchurch, M. J.: Application of satellite observations for timely updates to global anthropogenic NO_x emission inventories, *Geophys. Res. Lett.*, 38, L05810, doi:10.1029/2010gl046476, 2011.
- Leitão, J., Richter, A., Vrekoussis, M., Kokhanovsky, A., Zhang, Q. J., Beekmann, M., and Burrows, J. P.: On the improvement of NO₂ satellite retrievals – aerosol impact on the airmass factors, *Atmos. Meas. Tech.*, 3, 475–493, doi:10.5194/amt-3-475-2010, 2010.
- 15 Lin, J.-T.: Satellite constraint for emissions of nitrogen oxides from anthropogenic, lightning and soil sources over East China on a high-resolution grid, *Atmos. Chem. Phys.*, 12, 2881–2898, doi:10.5194/acp-12-2881-2012, 2012a.
- Lin, J. T. and McElroy, M. B.: Impacts of boundary layer mixing on pollutant vertical profiles in the lower troposphere: Implications to satellite remote sensing, *Atmos. Environ.*, 44, 1726–
20 1739, doi:10.1016/j.atmosenv.2010.02.009, 2010a.
- Lin, J.-T. and McElroy, M. B.: Detection from space of a reduction in anthropogenic emissions of nitrogen oxides during the Chinese economic downturn, *Atmos. Chem. Phys.*, 11, 8171–8188, doi:10.5194/acp-11-8171-2011, 2011.
- 25 Lin, J.-T., Nielsen, C. P., Zhao, Y., Lei, Y., Liu, Y., and McElroy, M. B.: Recent Changes in Particulate Air Pollution over China Observed from Space and the Ground: Effectiveness of Emission Control, *Environ. Sci. Technol.*, 44, 7771–7776, doi:10.1021/es101094t, 2010b.
- Lin, J.-T., McElroy, M. B., and Boersma, K. F.: Constraint of anthropogenic NO_x emissions in China from different sectors: a new methodology using multiple satellite retrievals, *Atmos. Chem. Phys.*, 10, 63–78, doi:10.5194/acp-10-63-2010, 2010c.
- 30 Lin, J.-T., Liu, Z., Zhang, Q., Liu, H., Mao, J., and Zhuang, G.: Modeling uncertainties for tropospheric nitrogen dioxide columns affecting satellite-based inverse modeling of nitrogen oxides emissions, *Atmos. Chem. Phys.*, 12, 12255–12275, doi:10.5194/acp-12-12255-2012, 2012b.

Retrieving
tropospheric nitrogen
dioxide over China

J.-T. Lin et al.

- Liu, J., Xia, X., Wang, P., Li, Z., Zheng, Y., Cribb, M., and Chen, H.: Significant aerosol direct radiative effects during a pollution episode in northern China, *Geophys. Res. Lett.*, 34, L23808, doi:10.1029/2007gl030953, 2007.
- Lucht, W., Schaaf, C. B., and Strahler, A. H.: An algorithm for the retrieval of albedo from space using semiempirical BRDF models, *IEEE T. Geosci. Remote*, 38, 977–998, doi:10.1109/36.841980, 2000.
- Ma, J. Z., Beirle, S., Jin, J. L., Shaiganfar, R., Yan, P., and Wagner, T.: Tropospheric NO₂ vertical column densities over Beijing: results of the first three years of ground-based MAX-DOAS measurements (2008–2011) and satellite validation, *Atmos. Chem. Phys.*, 13, 1547–1567, doi:10.5194/acp-13-1547-2013, 2013.
- Martin, R. V.: Satellite remote sensing of surface air quality, *Atmos. Environ.*, 42, 7823–7843, doi:10.1016/j.atmosenv.2008.07.018, 2008.
- Martin, R. V., Chance, K., Jacob, D. J., Kurosu, T. P., Spurr, R. J. D., Bucsela, E., Gleason, J. F., Palmer, P. I., Bey, I., Fiore, A. M., Li, Q. B., Yantosca, R. M., and Koelemeijer, R. B. A.: An improved retrieval of tropospheric nitrogen dioxide from GOME, *J. Geophys. Res.-Atmos.*, 107, 4437, doi:10.1029/2001jd001027, 2002.
- Martin, R. V., Jacob, D. J., Chance, K., Kurosu, T. P., Palmer, P. I., and Evans, M. J.: Global inventory of nitrogen oxide emissions constrained by space-based observations of NO₂ columns, *J. Geophys. Res.*, 108, 4537, doi:10.1029/2003JD003453, 2003.
- Martin, R. V., Sioris, C. E., Chance, K., Ryerson, T. B., Bertram, T. H., Wooldridge, P. J., Cohen, R. C., J. Andy Neuman, Swanson, A., and Flocke, F. M.: Evaluation of space-based constraints on global nitrogen oxide emissions with regional aircraft measurements over and downwind of eastern North America, *J. Geophys. Res.*, 111, D15308, doi:10.1029/2005JD006680, 2006.
- Mebust, A. K., Russell, A. R., Hudman, R. C., Valin, L. C., and Cohen, R. C.: Characterization of wildfire NO_x emissions using MODIS fire radiative power and OMI tropospheric NO₂ columns, *Atmos. Chem. Phys.*, 11, 5839–5851, doi:10.5194/acp-11-5839-2011, 2011.
- Mijling, B. and van der A, R. J.: Using daily satellite observations to estimate emissions of short-lived air pollutants on a mesoscopic scale, *J. Geophys. Res.-Atmos.*, 117, D17302, doi:10.1029/2012jd017817, 2012.
- Mijling, B., van der A, R. J., Boersma, K. F., Van Roozendael, M., De Smedt, I., and Kelder, H. M.: Reductions of NO₂ detected from space during the 2008 Beijing Olympic Games, *Geophys. Res. Lett.*, 36, D13801, doi:10.1029/2009gl038943, 2009.

Title Page	
Abstract	Introduction
Conclusions	References
Tables	Figures
◀	▶
◀	▶
Back	Close
Full Screen / Esc	
Printer-friendly Version	
Interactive Discussion	



Murray, L. T., Jacob, D. J., Logan, J. A., Hudman, R. C., and Koshak, W. J.: Optimized regional and interannual variability of lightning in a global chemical transport model constrained by LIS/OTD satellite data, *J. Geophys. Res.-Atmos.*, 117, D20307, doi:10.1029/2012jd017934, 2012.

5 Novotny, E. V., Bechle, M. J., Millet, D. B., and Marshall, J. D.: National Satellite-Based Land-Use Regression: NO_x in the United States, *Environ. Sci. Technol.*, 45, 4407–4414, doi:10.1021/es103578x, 2011.

10 O'Byrne, G., Martin, R. V., van Donkelaar, A., Joiner, J., and Celarier, E. A.: Surface reflectivity from the Ozone Monitoring Instrument using the Moderate Resolution Imaging Spectroradiometer to eliminate clouds: effects of snow on ultraviolet and visible trace gas retrievals, *J. Geophys. Res.-Atmos.*, 115, D17305, doi:10.1029/2009jd013079, 2010.

15 Ott, L. E., Pickering, K. E., Stenchikov, G. L., Allen, D. J., DeCaria, A. J., Ridley, B., Lin, R.-F., Lang, S., and Tao, W.-K.: Production of lightning NO_x and its vertical distribution calculated from three-dimensional cloud-scale chemical transport model simulations, *J. Geophys. Res.-Atmos.*, 115, D04301, doi:10.1029/2009jd011880, 2010.

20 Palmer, P. I., Jacob, D. J., Chance, K., Martin, R. V., Spurr, R. J. D., Kurosu, T. P., Bey, I., Yantosca, R., Fiore, A., and Li, Q. B.: Air mass factor formulation for spectroscopic measurements from satellites: application to formaldehyde retrievals from the Global Ozone Monitoring Experiment, *J. Geophys. Res.-Atmos.*, 106, 14539–14550, doi:10.1029/2000jd900772, 2001.

Park, R. J., Jacob, D. J., Chin, M., and Martin, R. V.: Sources of carbonaceous aerosols over the United States and implications for natural visibility, *J. Geophys. Res.-Atmos.*, 108, 4355, doi:10.1029/2002jd003190, 2003.

25 Park, R. J., Jacob, D. J., Field, B. D., Yantosca, R. M., and Chin, M.: Natural and transboundary pollution influences on sulfate-nitrate-ammonium aerosols in the US: implications for policy, *J. Geophys. Res.-Atmos.*, 109, D15204, doi:10.1029/2003jd004473, 2004.

30 Park, R. J., Jacob, D. J., Kumar, N., and Yantosca, R. M.: Regional visibility statistics in the United States: natural and transboundary pollution influences, and implications for the Regional Haze Rule, *Atmos. Environ.*, 40, 5405–5423, doi:10.1016/j.atmosenv.2006.04.059, 2006.

Price, C., Penner, J., and Prather, M.: NO_x from lightning, 1, global distribution based on lightning physics, *J. Geophys. Res.*, 102, 5929–5941, doi:10.1029/96JD03504, 1997.

Retrieving tropospheric nitrogen dioxide over China

J.-T. Lin et al.

[Title Page](#)

[Abstract](#)

[Introduction](#)

[Conclusions](#)

[References](#)

[Tables](#)

[Figures](#)

◀

▶

◀

▶

[Back](#)

[Close](#)

[Full Screen / Esc](#)

[Printer-friendly Version](#)

[Interactive Discussion](#)



- Remer, L. A., Kleidman, R. G., Levy, R. C., Kaufman, Y. J., Tanre, D., Mattoo, S., Martins, J. V., Ichoku, C., Koren, I., Yu, H. B., and Holben, B. N.: Global aerosol climatology from the MODIS satellite sensors, *J. Geophys. Res.-Atmos.*, 113, D14s07, doi:10.1029/2007jd009661, 2008.
- Richter, A., Burrows, J. P., Nüß, H., Granier, C., and Niemeier, U.: Increase in tropospheric nitrogen dioxide over China observed from space, *Nature*, 437, 129–132, doi:10.1038/nature04092, 2005.
- Rienecker, M. M., Suarez, M. J., Todling, R., Bacmeister, J., Takacs, L., Liu, H.-C., Gu, W., Sienkiewicz, M., Koster, R. D., Gelaro, R., Stajner, I., and Nielsen, E.: The GEOS-5 Data Assimilation System – Documentation of Versions 5.0.1, 9.1.0, and 5.2.0, NASA, 2008.
- Rodgers, C. D.: Inverse Methods for Atmospheric Sounding: Theory and Practice, World Scientific Publishing, Singapore-New Jersey-London-Hong Kong, 2000.
- Russell, A. R., Perring, A. E., Valin, L. C., Bucsela, E. J., Browne, E. C., Wooldridge, P. J., and Cohen, R. C.: A high spatial resolution retrieval of NO₂ column densities from OMI: method and evaluation, *Atmos. Chem. Phys.*, 11, 8543–8554, doi:10.5194/acp-11-8543-2011, 2011.
- Sauvage, B., Martin, R. V., van Donkelaar, A., Liu, X., Chance, K., Jaeglé, L., Palmer, P. I., Wu, S., and Fu, T.-M.: Remote sensed and in situ constraints on processes affecting tropical tropospheric ozone, *Atmos. Chem. Phys.*, 7, 815–838, doi:10.5194/acp-7-815-2007, 2007.
- Sluis, W. W., Allaart, M. A. F., Piters, A. J. M., and Gast, L. F. L.: The development of a nitrogen dioxide sonde, *Atmos. Meas. Tech.*, 3, 1753–1762, doi:10.5194/amt-3-1753-2010, 2010.
- Sneep, M., de Haan, J. F., Stammes, P., Wang, P., Vanbauce, C., Joiner, J., Vasilkov, A. P., and Levelt, P. F.: Three-way comparison between OMI and PARASOL cloud pressure products, *J. Geophys. Res.-Atmos.*, 113, D15s23, doi:10.1029/2007jd008694, 2008.
- Spurr, R.: LIDORT and VLIDORT: Linearized pseudo-spherical scalar and vector discrete ordinate radiative transfer models for use in remote sensing retrieval problems, in: Light Scattering Reviews, edited by: Kokhanovsky, A., Springer, 2008.
- van Donkelaar, A., Martin, R. V., Spurr, R. J. D., Drury, E., Remer, L. A., Levy, R. C., and Wang, J.: Optimal estimation for global ground-level fine particulate matter concentrations, *J. Geophys. Res.-Atmos.*, 118, 5621–5636, doi:10.1002/jgrd.50479, 2013.
- Walker, T. W., Martin, R. V., van Donkelaar, A., Leaitch, W. R., MacDonald, A. M., Anlauf, K. G., Cohen, R. C., Bertram, T. H., Huey, L. G., Avery, M. A., Weinheimer, A. J., Flocke, F. M., Tarasick, D. W., Thompson, A. M., Streets, D. G., and Liu, X.: Trans-Pacific transport of reactive nitrogen and ozone to Canada during spring, *Atmos. Chem. Phys.*, 10, 8353–8372, doi:10.5194/acp-10-8353-2010, 2010.

Title Page	
Abstract	Introduction
Conclusions	References
Tables	Figures
◀	▶
◀	▶
Back	Close
Full Screen / Esc	
Printer-friendly Version	
Interactive Discussion	



Retrieving tropospheric nitrogen dioxide over China

J.-T. Lin et al.

- Wang, J., Xu, X., Spurr, R., Wang, Y., and Drury, E.: Improved algorithm for MODIS satellite retrievals of aerosol optical thickness over land in dusty atmosphere: implications for air quality monitoring in China, *Remote Sens. Environ.*, 114, 2575–2583, doi:10.1016/j.rse.2010.05.034, 2010.
- 5 Wang, S. W., Zhang, Q., Streets, D. G., He, K. B., Martin, R. V., Lamsal, L. N., Chen, D., Lei, Y., and Lu, Z.: Growth in NO_x emissions from power plants in China: bottom-up estimates and satellite observations, *Atmos. Chem. Phys.*, 12, 4429–4447, doi:10.5194/acp-12-4429-2012, 2012.
- 10 Wang, X., Wang, Y., Hao, J., Kondo, Y., Irwin, M., Munger, J. W., and Zhao, Y.: Top-down estimate of China's black carbon emissions using surface observations: sensitivity to observation representativeness and transport model error, *J. Geophys. Res.-Atmos.*, 118, 5781–5795, doi:10.1002/jgrd.50397, 2013.
- 15 Wang, Y., Jacob, D. J., and Logan, J. A.: Global simulation of tropospheric O₃-NO_x-hydrocarbon chemistry. 1. Model formulation, *J. Geophys. Res.*, 103, 10713–10725, 1998.
- 20 Yang, F., Tan, J., Zhao, Q., Du, Z., He, K., Ma, Y., Duan, F., Chen, G., and Zhao, Q.: Characteristics of PM_{2.5} speciation in representative megacities and across China, *Atmos. Chem. Phys.*, 11, 5207–5219, doi:10.5194/acp-11-5207-2011, 2011.
- 25 Yienger, J. J. and Levy, H.: Empirical model of global soil-biogenic NO_x emissions, *J. Geophys. Res.*, 100, 11447–11464, 1995.
- 30 Yu, H., Wang, P., Zong, X., Li, X., and Lue, D.: Change of NO₂ column density over Beijing from satellite measurement during the Beijing 2008 Olympic Games, *Chinese Sci. Bull.*, 55, 308–313, doi:10.1007/s11434-009-0375-0, 2010.
- Zender, C. S., Bian, H. S., and Newman, D.: Mineral Dust Entrainment and Deposition (DEAD) model: description and 1990s dust climatology, *J. Geophys. Res.-Atmos.*, 108, 4416, doi:10.1029/2002jd002775, 2003.
- 35 Zhang, Q., Streets, D. G., Carmichael, G. R., He, K. B., Huo, H., Kannari, A., Klimont, Z., Park, I. S., Reddy, S., Fu, J. S., Chen, D., Duan, L., Lei, Y., Wang, L. T., and Yao, Z. L.: Asian emissions in 2006 for the NASA INTEX-B mission, *Atmos. Chem. Phys.*, 9, 5131–5153, doi:10.5194/acp-9-5131-2009, 2009.
- 40 Zhang, Q., He, K. B., and Huo, H.: Cleaning China's air, *Nature*, 484, 161–162, 2012.
- Zhao, C. and Wang, Y. H.: Assimilated inversion of NO_x emissions over east Asia using OMI NO₂ column measurements, *Geophys. Res. Lett.*, 36, L06805, doi:10.1029/2008gl037123, 2009.

Title Page	
Abstract	Introduction
Conclusions	References
Tables	Figures
◀	▶
◀	▶
Back	Close
Full Screen / Esc	
Printer-friendly Version	
Interactive Discussion	



Zhou, Y., Brunner, D., Spurr, R. J. D., Boersma, K. F., Sneep, M., Popp, C., and Buchmann, B.: Accounting for surface reflectance anisotropy in satellite retrievals of tropospheric NO₂, *Atmos. Meas. Tech.*, 3, 1185–1203, doi:10.5194/amt-3-1185-2010, 2010.

Zhou, Y. P., Brunner, D., Hueglin, C., Henne, S., and Staehelin, J.: Changes in OMI tropospheric NO₂ columns over Europe from 2004 to 2009 and the influence of meteorological variability, *Atmos. Environ.*, 46, 482–495, doi:10.1016/j.atmosenv.2011.09.024, 2012.

Retrieving tropospheric nitrogen dioxide over China

J.-T. Lin et al.

[Title Page](#)

[Abstract](#)

[Introduction](#)

[Conclusions](#)

[References](#)

[Tables](#)

[Figures](#)

◀

▶

[Back](#)

[Close](#)

[Full Screen / Esc](#)

[Printer-friendly Version](#)

[Interactive Discussion](#)



**Retrieving
tropospheric nitrogen
dioxide over China**

J.-T. Lin et al.

Table 1. MAX-DOAS measurements.

Location	Spatial Information	Measurement Time	Reference
Tai'An	117.15° E, 36.16° N, 126 m; urban	30 May–29 Jun 2006	Irie et al., 2012
IAP	116.38° E, 39.98° N, 92 m; urban	22 Jun 2008–16 Apr 2009	Hendrick et al., 2013
Xianghe	116.96° E, 39.75° N, 36 m; suburban	29 Sep –15 Oct 2011	Hendrick et al., 2013

[Title Page](#)[Abstract](#)[Introduction](#)[Conclusions](#)[References](#)[Tables](#)[Figures](#)[Back](#)[Close](#)[Full Screen / Esc](#)[Printer-friendly Version](#)[Interactive Discussion](#)

Retrieving tropospheric nitrogen dioxide over China

J.-T. Lin et al.

Table 2. RTMs and ancillary parameters in deriving tropospheric NO₂ columns from OMI.

	DOMINO-2	Our Reference Retrieval (Case 0 in Table 4)
RTM	DAK v3.0	LIDORT v3.6
Surface reflectance	OMLER v1 (3 yr average; 0.5°)	BRDF; MCD43C2 Collection 5 (0.05°)
Surface pressure	TM4 (3° lon × 2° lat); adjusted by elevation	GEOS-Chem (0.667° lon × 0.5° lat); adjusted by elevation
Cloud fraction	OMCLDO2 v1.1.1.3; by look-up table	Derived here
Cloud pressure	OMCLDO2 v1.1.1.3; by look-up table	Derived here
Aerosol optics	Treated implicitly as “effective” clouds	GEOS-Chem simulations;
Pressure levels, temperature profile, and NO ₂ vertical profile	TM4 (3° lon × 2° lat; 34 layers)*	AOD is adjusted by AERONET, MAX-DOAS or MODIS GEOS-Chem (0.667° lon × 0.5° lat; 47 layers)*
Calculation for individual pixels	Interpolated from a look-up table	Pixel-specific radiative transfer modeling; no look-up table

*The pressure levels are re-calculated according to the elevation-adjusted surface pressure; while the VMRs of NO₂ are not changed in individual layers (Zhou et al., 2009).

- [Title Page](#)
- [Abstract](#) [Introduction](#)
- [Conclusions](#) [References](#)
- [Tables](#) [Figures](#)
- [◀](#) [▶](#)
- [◀](#) [▶](#)
- [Back](#) [Close](#)
- [Full Screen / Esc](#)
- [Printer-friendly Version](#)
- [Interactive Discussion](#)



Retrieving tropospheric nitrogen dioxide over China

J.-T. Lin et al.

Table 3. RTMs and ancillary parameters in deriving cloud properties from OMI.

	OMCLDO2 v1.1.1.3	Our Reference Retrieval (wrt Case 0 in Table 4)
RTM	DAK v3.0	LIDORT v3.6
Surface reflectance	OMLER v1 (3 yr average; 0.5°)	BRDF; MCD43C2 Collection 5 (0.05°)
Surface pressure	Interpolated from a fixed pressure–height relation (midlatitude summer profile)	GEOS-Chem (0.667° lon × 0.5° lat); adjusted by elevation
Aerosol optics	No aerosols	GEOS-Chem simulations; AOD is adjusted by AERONET, MAX-DOAS or MODIS
Pressure levels and temperature profile	Fixed dependence on height (midlatitude summer profile)	GEOS-Chem (0.667° lon × 0.5° lat; 47 layers)*
Calculation for individual pixels	Interpolated from a look-up table	Pixel-specific radiative transfer modeling; no look-up table

*The pressure levels are re-calculated according to the elevation-adjusted surface pressure.

- [Title Page](#)
- [Abstract](#) | [Introduction](#)
- [Conclusions](#) | [References](#)
- [Tables](#) | [Figures](#)
- [◀](#) | [▶](#)
- [◀](#) | [▶](#)
- [Back](#) | [Close](#)
- [Full Screen / Esc](#)
- [Printer-friendly Version](#)
- [Interactive Discussion](#)



Retrieving tropospheric nitrogen dioxide over China

J.-T. Lin et al.

[Title Page](#)

[Abstract](#)

[Introduction](#)

[Conclusions](#)

[References](#)

[Tables](#)

[Figures](#)

◀

▶

◀

▶

[Back](#)

[Close](#)

[Full Screen / Esc](#)

[Printer-friendly Version](#)

[Interactive Discussion](#)

Table 4. Retrieving VCDs of NO₂ from OMI by altering the ancillary parameters.

Case	Tested parameter	Differences from our reference retrieval (Case 0)
0		Reference retrieval
1		Mimicking DOMINO-2, but not using the LUT
2		Mimicking DOMINO-2, but adopting surface pressure from OMCLDO2 and not using the LUT
3	Surface reflectance	Using blue-sky surface albedo derived from MODIS BRDF
4	Surface reflectance	Using black-sky surface albedo derived from MODIS BRDF
5	Surface reflectance	Using 5 yr average surface albedo from OMI (OMLER v3)
6	Surface reflectance	Using 3 yr average surface albedo from OMI; as in DOMINO-2
7	NO ₂ profile	Adopting vertical profiles of NO ₂ VMRs from MAX-DOAS
8	NO ₂ profile	Adopting vertical profiles of NO ₂ VMRs from TM4
9	NO ₂ profile	Assuming an exponential decrease of NO ₂ VMRs from surface to 1.5 km with a scale height of 0.25 km
10	NO ₂ profile	Assuming constant VMR of NO ₂ from surface to 1.5 km
11	NO ₂ profile	Assuming an exponential decrease of NO ₂ VMRs from surface to 3.0 km with a scale height of 0.25 km
12	AOD	Assuming no AOD
13	Aerosol absorption	Assuming no aerosol absorption
14	Aerosol absorption	Doubling aerosol absorption
15	Aerosol profile	Assuming constant aerosol extinction coefficient in the troposphere
16	Aerosol profile	Putting all tropospheric aerosols at the PBL top
17	Aerosol profile	Putting all tropospheric aerosols at the tropopause



**Retrieving
tropospheric nitrogen
dioxide over China**

J.-T. Lin et al.

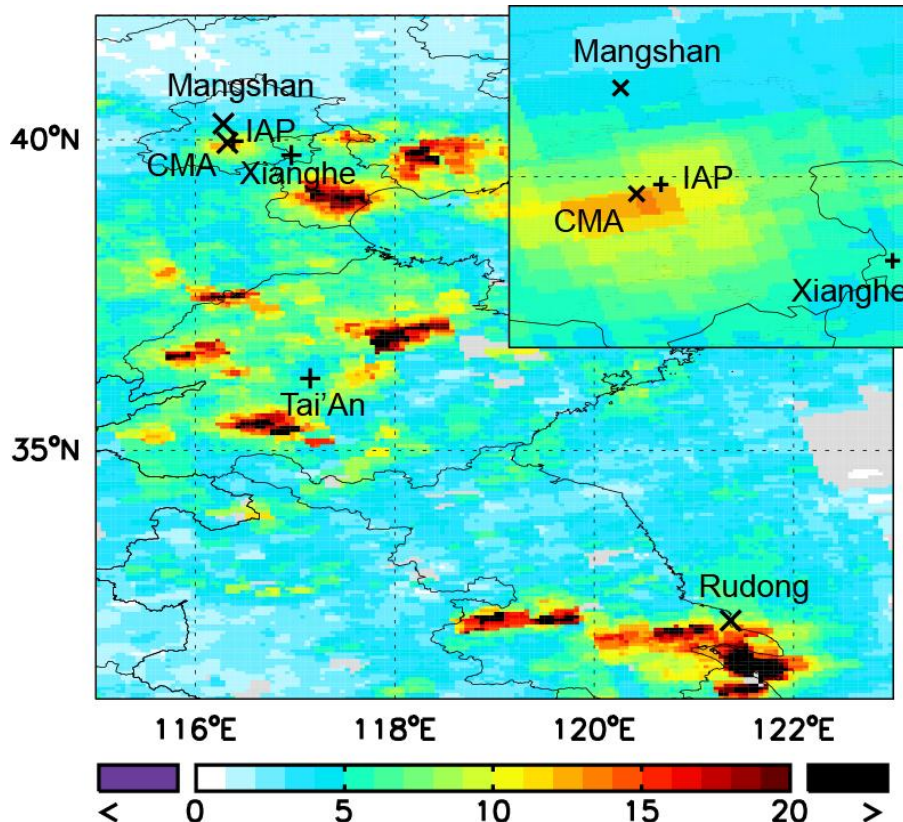


Fig. 1. Sites of MAX-DOAS measurements used in this study (Beijing IAP, Xianghe and Tai'An; "+" signs) and in previous studies (Mangshan, Rudong (Irie et al., 2012) and Beijing CMA (Ma et al., 2013); "x" signs). Overlaid on the background is the spatial distribution of NO₂ columns (10^{15} molec. cm⁻²; at 0.05°) in July 2008 retrieved by DOMINO-2 together with a zoom-in map around Beijing (116°–117° E, 39.5°–40.5° N; at 0.01°). OMI pixels are restricted to row anomaly free, ice/snow free, CRF \leq 0.5, and VZA \leq 30°.

- [Title Page](#)
- [Abstract](#) [Introduction](#)
- [Conclusions](#) [References](#)
- [Tables](#) [Figures](#)
- [◀](#) [▶](#)
- [◀](#) [▶](#)
- [Back](#) [Close](#)
- [Full Screen / Esc](#)
- [Printer-friendly Version](#)
- [Interactive Discussion](#)

Retrieving tropospheric nitrogen dioxide over China

J.-T. Lin et al.

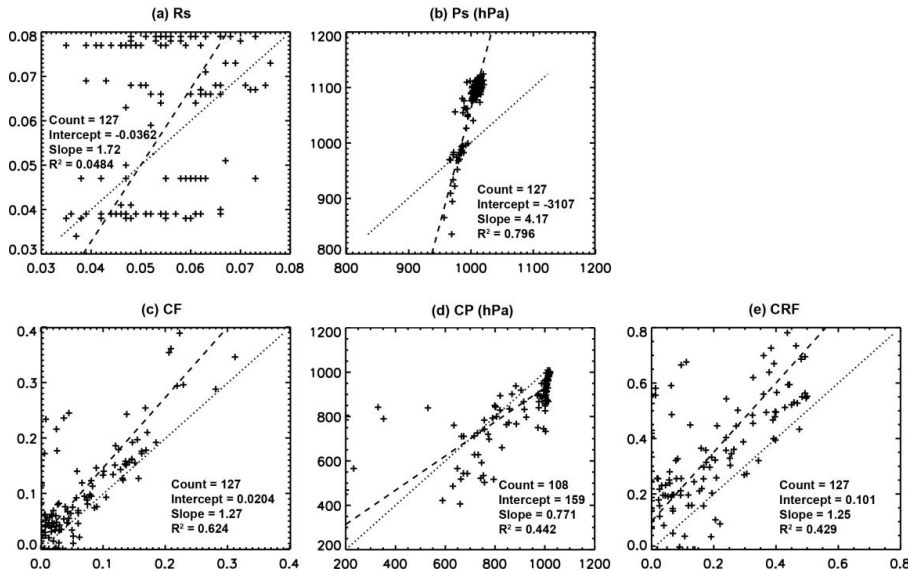


Fig. 2. Scatter plots between DOMINO-2 (y-axis) and our reference retrieval (x-axis) for Rs, Ps, CF, CP and CRF across the individual pixels. For **(a)**, the OMLER v1 albedo data (y-axis) are compared to the MODIS bi-directional reflectance factors (BRF; x-axis). The criteria for pixel selection are presented in Sect. 2.4. The number of pixels is smaller for CP because CF = 0 in some pixels. Also shown is the statistics from the RMA regression; the dashed line indicates the regression curve and the dotted line denotes the 1 : 1 relationship.

Retrieving tropospheric nitrogen dioxide over China

J.-T. Lin et al.

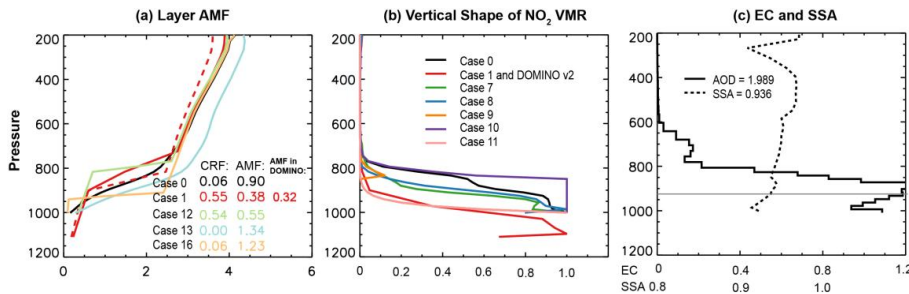


Fig. 3. (a) The pressure dependence of layer AMFs for an OMI pixel on 28 December 2008. The derived CRF and AMF are depicted as well, together with the AMF from DOMINO-2 (with respect to the red dashed line). (b) The vertical shape of NO_2 (i.e., VMRs of NO_2 normalized to the maximum VMR). (c) The vertical profiles of aerosol extinction coefficient (EC; km^{-1}) and SSA assumed in our reference retrieval (Case 0). The thickness of the individual layers is shown in the EC line. The horizontal grey line depicts the top of the PBL.

Title Page	Abstract	Introduction
Conclusions	References	
Tables	Figures	
◀	▶	
◀	▶	
Back	Close	
Full Screen / Esc		
Printer-friendly Version		
Interactive Discussion		



Retrieving tropospheric nitrogen dioxide over China

J.-T. Lin et al.

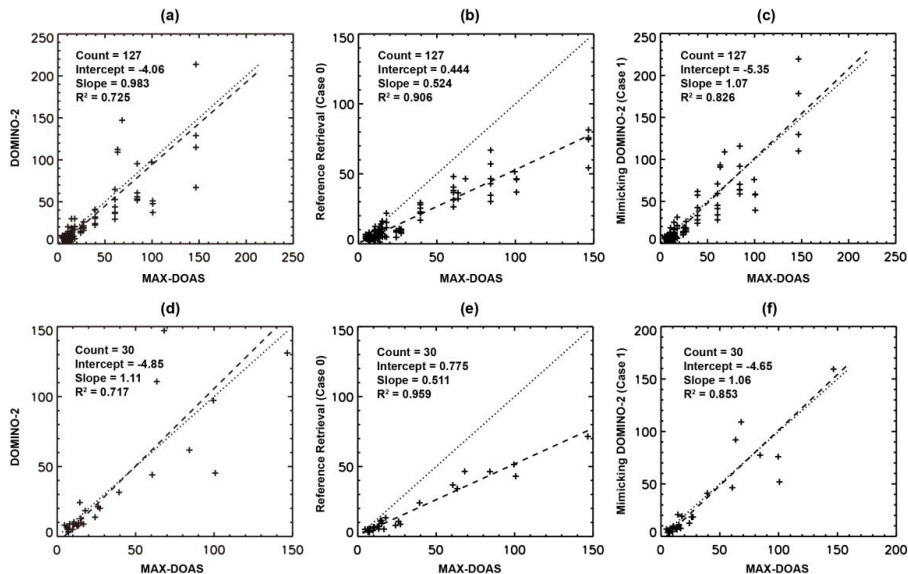


Fig. 4. Scatter plots for NO_2 columns ($10^{15} \text{ molec cm}^{-2}$) from MAX-DOAS measurements and OMI retrievals. Each “+” corresponds to an OMI pixel in (a–c), and to the mean value from all OMI pixels in a day in (d–f). The criteria for pixel selection are presented in Sect. 2.4. Also shown is the statistics from the RMA regression; the dashed line indicates the regression curve and the dotted line denotes the $1 : 1$ relationship. The RMA regression in (a–c) should be interpreted with caution since there may be multiple OMI pixels/data in a day corresponding to a single MAX-DOAS value.

Title Page	Abstract	Introduction
Conclusions	References	
Tables	Figures	
◀	▶	
◀	▶	
Back	Close	
Full Screen / Esc		
Printer-friendly Version		
Interactive Discussion		



**Retrieving
tropospheric nitrogen
dioxide over China**

J.-T. Lin et al.

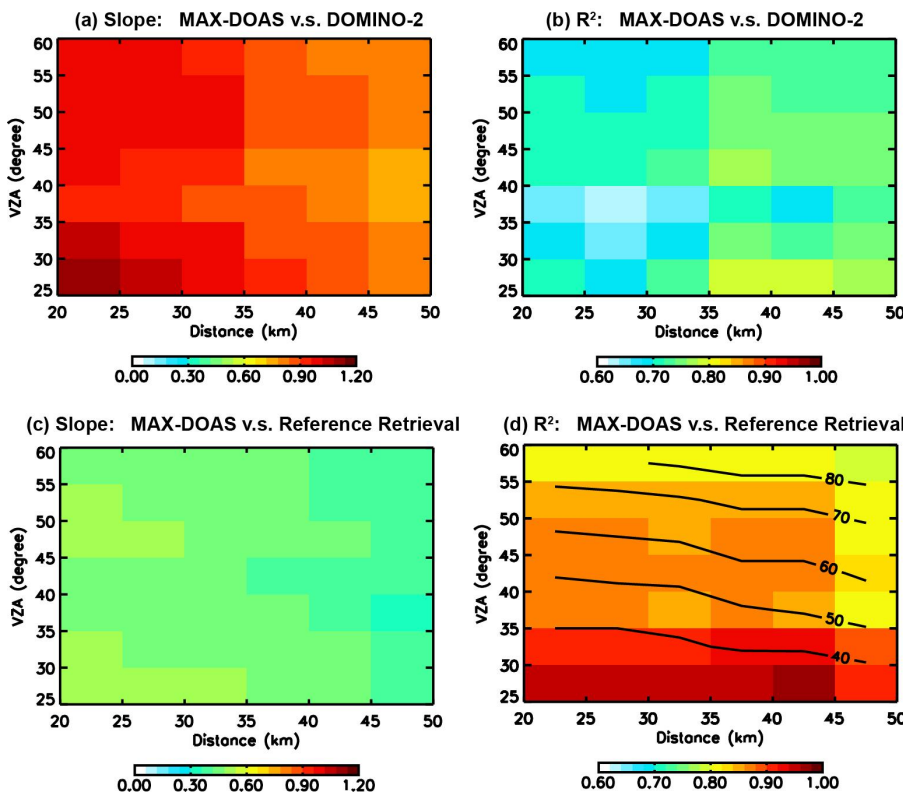


Fig. 5. Dependence on pixel-center distance and VZA of the RMA regression (slope and R^2) for the daily NO_2 columns between MAX-DOAS and OMI retrievals. The lower left tile in each panel represents distance $\leq 25 \text{ km}$ and VZA $\leq 30^\circ$. VZA $\leq 60^\circ$ means no limitation since the VZA never exceeds 57° . The rest criteria for pixel section are not changed. Overlaid on (d) is the number of days with suitable NO_2 data for conducting the RMA regression.

Retrieving tropospheric nitrogen dioxide over China

J.-T. Lin et al.

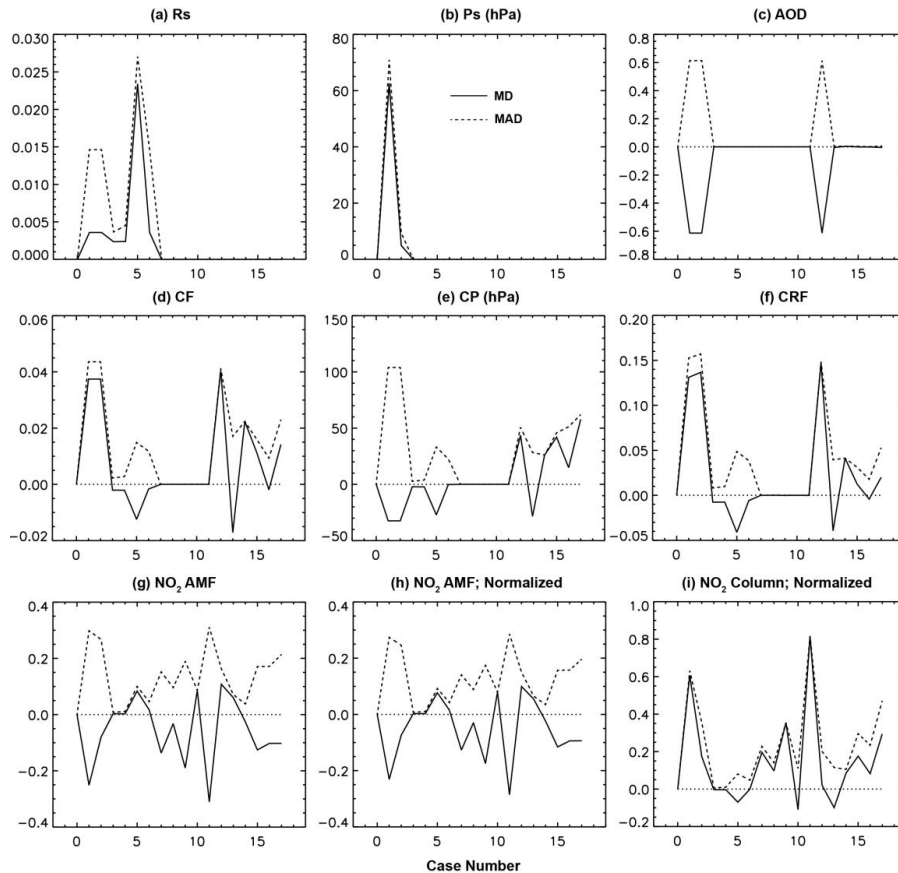


Fig. 6. (a–g) The mean difference (MD) and mean absolute difference (MAD) across the selected 127 pixels between our OMI retrievals (Cases 0–17) and our reference retrieval (Case 0). **(h, i)** The normalized mean difference (NMD) and normalized mean absolute difference (NMAD). The criteria for pixel selection are presented in Sect. 2.4.

**Retrieving
tropospheric nitrogen
dioxide over China**

J.-T. Lin et al.

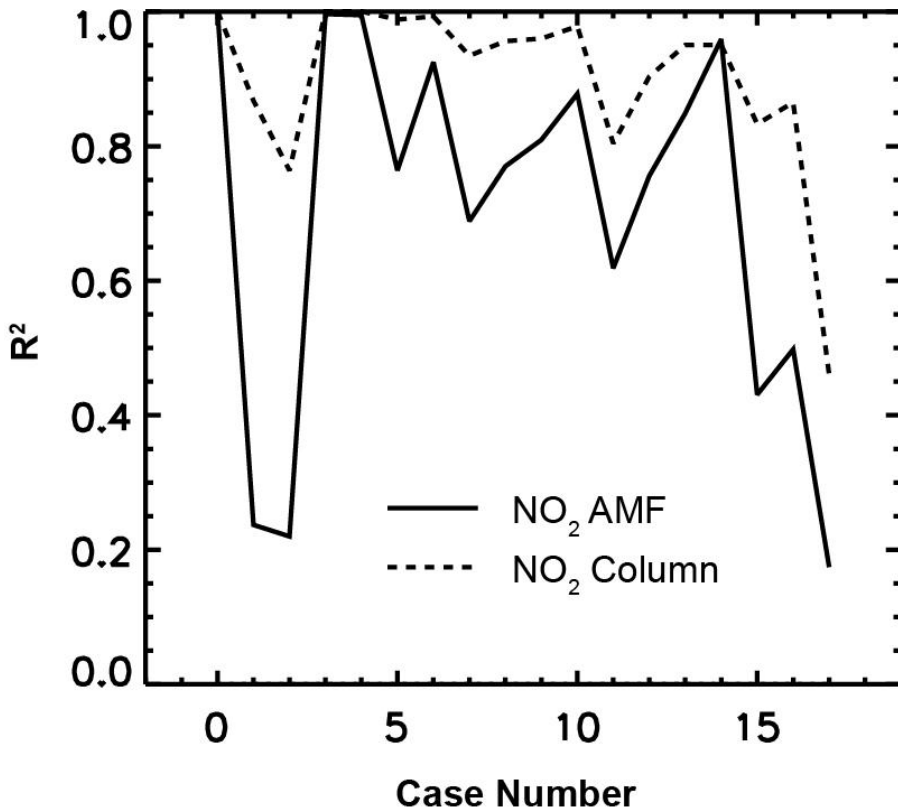


Fig. 7. The R^2 between Cases 0–17 and our reference retrieval (Case 0) across the selected 127 OMI pixels for the AMF and VCD of NO_2 . The criteria for pixel selection are presented in Sect. 2.4.

Retrieving tropospheric nitrogen dioxide over China

J.-T. Lin et al.

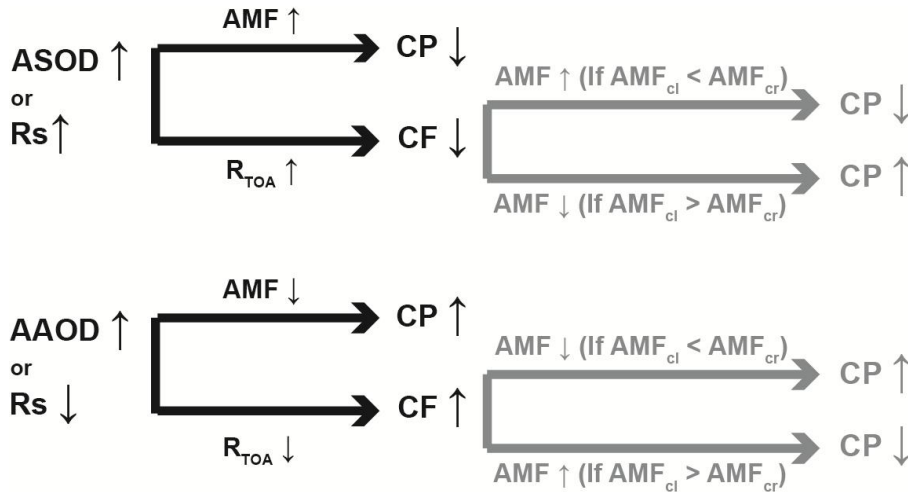


Fig. 8. Effects of Rs, ASOD and AAOD on the retrieval of CF and CP. Aerosols are assumed to be concentrated in the lower troposphere, as for the 127 pixels examined in this study. The grey color denotes a secondary effect of the changed CF on the CP; the effect depends on the amount of O₂-O₂ AMF for the cloudy portion of the pixel (AMF_{cl}) relative to the AMF for the clear-sky portion (AMF_{cr}). The changes in CP have a relatively small effect on the CF (not depicted here).

Retrieving tropospheric nitrogen dioxide over China

J.-T. Lin et al.

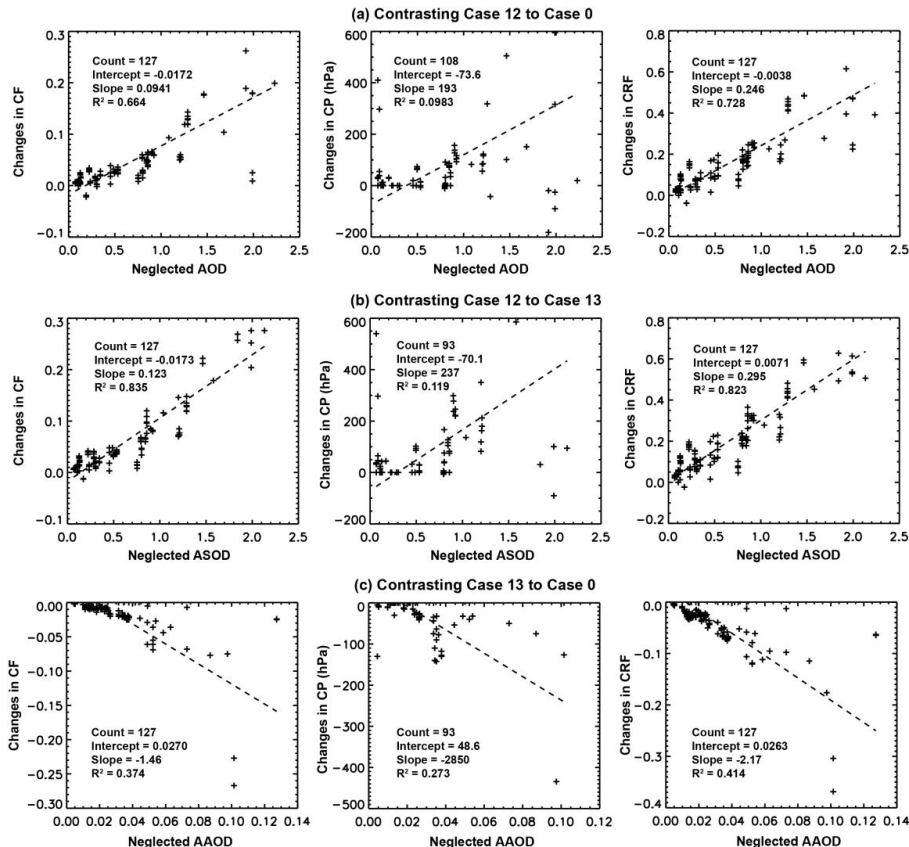


Fig. 9. Changes in the retrieved CF, CP and CRF for the 127 OMI pixels by neglecting **(a)** AOD, **(b)** aerosol scattering, and **(c)** aerosol absorption. The criteria for pixel selection are presented in Sect. 2.4. The number of pixels is smaller for CP because CF = 0 in some pixels. Also shown is the statistics from the RMA regression; the dashed line indicates the regression curve.

Retrieving tropospheric nitrogen dioxide over China

J.-T. Lin et al.

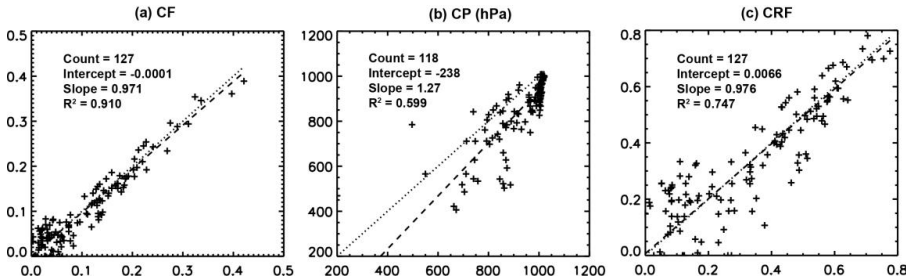


Fig. 10. Scatter plots between DOMINO-2 (y-axis) and our Case 12 (no aerosols; x-axis) for CF, CP and CRF across the individual pixels. DOMINO-2 adopts CF and CP from OMCLDO2. The criteria for pixel selection are presented in Sect. 2.4. The number of pixels is smaller for CP because CF = 0 in some pixels. Also shown is the statistics from the RMA regression; the dashed line indicates the regression curve and the dotted line denotes the 1 : 1 relationship.

Retrieving tropospheric nitrogen dioxide over China

J.-T. Lin et al.

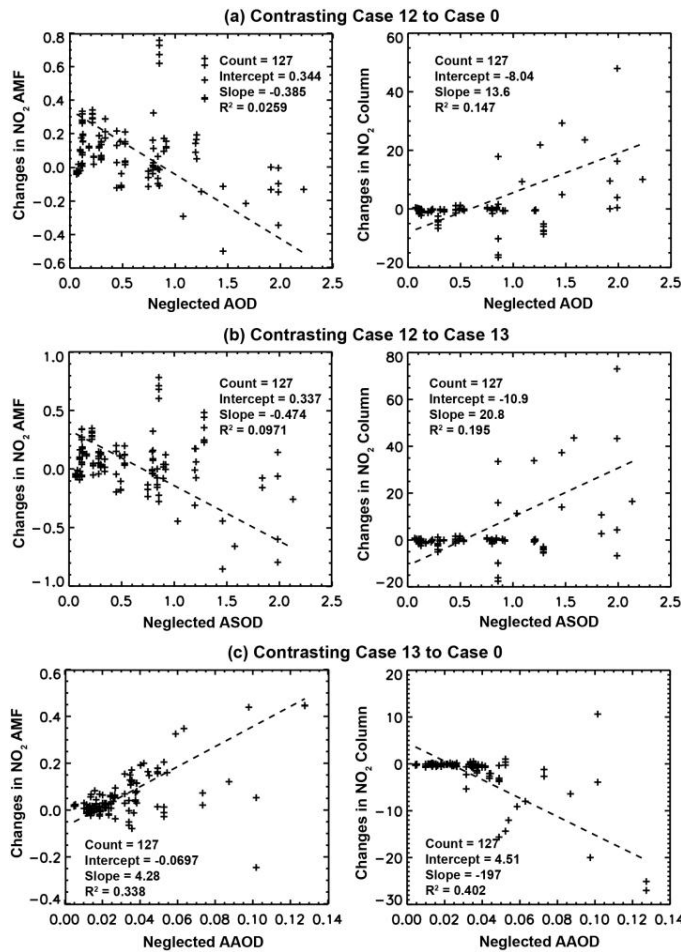


Fig. 11. Similar to Fig. 9 but for the AMF and VCD of NO₂.

**Retrieving
tropospheric nitrogen
dioxide over China**

J.-T. Lin et al.

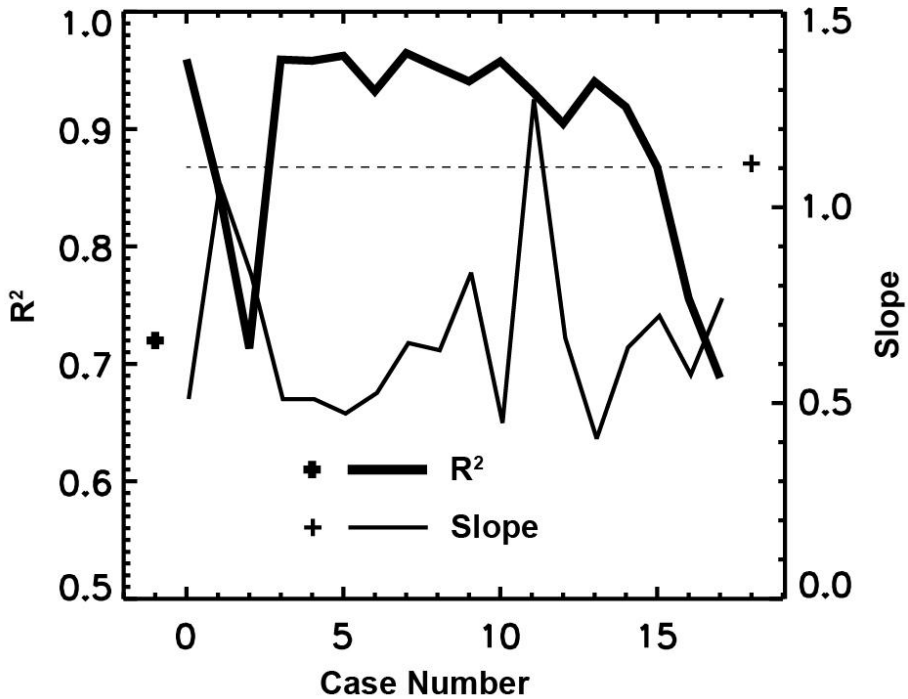


Fig. 12. The slope and R^2 of the RMA regression for daily NO₂ columns between our OMI retrievals and MAX-DOAS measurements. The criteria for pixel selection are presented in Sect. 2.4. The thick and thin "+" signs represent the respective results when pairing DOMINO-2 with MAX-DOAS. The horizontal dashed line denotes the R^2 between MAX-DOAS VCD and OMI gVCD (see Sect. 4).